To the Graduate Council:

I am submitting herewith a thesis written by Peter P. Engar, Jr. entitled "Quantitative Determination of the Fraction of Rydberg Electrons in a Convoy Electron Cusp." I have examined the final copy of this thesis for form and content and recommend that it be accepted in partial fulillment of the requirements for the degree of Master of Science, with a major in Physics.

Ivan A. Sellin, Major Professor

We have read this thesis
and recommend its acceptance

Marianne Breinig

W. E. Deeds

Accepted for the Council:

Vice Provost
and Dean of the Graduate School

STATEMENT OF PERMISSION TO USE

In presenting this thesis in partial fulfillment of the requirments for a Master's degree at the University of Tennessee, Knoxville, I agree that the Library shall make it available to borrowers under rules of the Library. Brief quotations from this thesis are allowable without special permission, provided that accurate acknowledgment of the source is made.

Permission for extensive quotation from or reproduction of this thesis may be granted by my major professor, or in his absence, by the Head of Interlibrary Services when, in the opinion of either, the proposed use of the material is for scholalry purposes. Any copying or use of the material in this thesis for financial gain shall not be allowed without my written permission.

Signature Peter Paul Engargh

Date June 14, 1985

QUANTITIVE DETERMINATION OF THE FRACTION OF RYDBERG ELECTRONS IN A CONVOY ELECTRON CUSP

A Thesis

Presented for the

Master of Science

Degree

The University of Tennessee, Knoxville

Peter P. Engar, Jr.

August 1985

DEDICATED TO MY PARENTS

ACKNOWLEDGEMENTS

I wish to express my gratitude to the entire Atomic Physics Group at The University of Tennessee and the staff of the ORNL EN Tandem Van de Graaff facility for their many long hours of assistance.

I would like to thank our group's secretary, B.G. for her expert help in the preparation of the thesis and my fellow students for their support. I especially would like to thank Dr. Marianne Breinig, whose guidance and assitance made this project possible. Finally, I wish to thank my parents for their constant encouragement.

ABSTRACT

Convoy electron energy spectra were measured using an electrostatic electron energy analyzer and CEM detector. Recently it was suggested that the origin of a significant fraction of the measured convoy electron yields is due to field ionization of high Rydberg states inside the electron energy analyzer.

Using the ORNL EN Tandem Van De Graaff accelerator, beams of 18 MeV O^{+3} and 32 MeV O^{+5} ions were passed either through a foil target in the focus of the analyzer or through a foil target out of focus and then through a series of field ionization and deflection plates, before entering the electrostatic electron energy analyzer. Various voltages were applied across the different plates. Yields of energy analyzed electrons were obtained for different geometric arrangements of the plates and for different combinations of the electric fields.

The data indicate that the contribution of field ionized Rydbergs electrons to convoy yields is small, less than 3% in traditional experiments designed to study convoy electrons. The measured yields as a function of the applied electric field between the ionization plates are consistent with a quantum state population P(n) of highly excited states varying as n^{-3}. No indication of strong alignment of these highly excited states is found when comparing the effectiveness in field ionization of a transverse vs a longitudinal field.

TABLE OF CONTENTS

CHAPTER		PAGE
I.	INTRODUCTION	1
	A. The Beam Foil Interaction	
	B. Foil Excited Rydberg States	
	C. Convoy Electrons	
	D. Present Dispute	
II.	APPARATUS AND EXPERIMENTAL METHOD	21
	A. Beam Line Sections	
	B. Experimental Package	
	C. Electronics and Data Acquisition	
	D. Experimental Procedure	
III.	DATA ANALYSIS AND RESULTS	40
	A. Determination of Relative Electron Yields	
	B. Estimation of Quantum State Population P(n)	
	C. A Check on Enhanced Rydberg Electron Yield: Alignment	
	D. Quantum Beat Oscillations: Coherent Excitation	
IV.	DISCUSSION	57
	A. Current Dispute Examined	
	B. Quantum State Population P(n)	
	C. Nonstatistical Sublevel Populations	
LIST OF REFERENCES		62
VITA		65

LIST OF FIGURES

FIGURE		PAGE
1.	The Typical Setup for a Beam Foil Experiment	2
2.	The Various Aspects of a Foil	4
3.	Hypothetical Multi-step Model for the Formation of Rydberg States of Fast Ions Emerging from Solid Targets	10
4.	The Shape of the Saddle Point Potential Energy of Equation (1)	12
5.	Experimental Setup to Examine a Particular Band of Foil Excited Rydberg States	14
6.	A Typical Setup to Measure Electron Energy Distributions .	17
7.	The Various Parts of the Beamline	22
8.	Component Bench Assembly	24
9.	Foil Targets and Electrostatic Plates	27
10.	The Elements of a 180° Spherical Sector Electrostatic Analyzer with its Focusing Parameters	31
11.	The 160° Spherical Sector Analyzer and Experimental Setup .	33
12.	Block Diagram of Electronics	36
13.	Energy Distribution for Electrons Originating at a) The In Focus Target b) The Out Of Focus Target	42
14.	Electron Energy Distributions as a Function of a Deflection Field F_I Applied Perpendicular to the Beam	45
15.	Electron Yield from the Out Of Focus Target as a Function of Electric Field F_I	46
16.	The Shapes of Two Electron Cusps Measured with a) An Electric Field $F_I = 0$ and b) An Electric Field $F_I = 62.5$V/cm Perpendicular to the Beam Direction	47
17.	Yield of Rydberg Electrons Ionized in the Analyzer as a Function of F_I a) Perpendicular and b) Parallel to the Beam	50
18.	Oscillation in the Rydberg Yield as a Function of Ionization Field F_I	56

19. Experimental Setup Used by Vager Et Al. 58

CHAPTER I

INTRODUCTION

A. The Beam Foil Interaction

The fundamental aspects of the interaction of particles with solids are currently being investigated by scientists from a variety of disciplines such as particle physics, nuclear physics, atomic and molecular physics, solid state physics and surface physics.[1] The beam-foil interaction as a special case of the ion solid interaction is a problem of great interest in the field of atomic collision physics. What are the dominant interactions as fast ($E \geq 1$ MeV/u) heavy ($Z \geq 6$) ions pass through thin solid targets (typical target thickness 200-2000A)? In this thesis we investigate, using field ionization techniques, some of the properties of the excited states of heavy ions that are produced as a result of the interaction with a thin foil. Field ionization of highly excited states produces free electrons traveling with velocity $\vec{v}_e$ approximately equal to the ion velocity $\vec{v}$. In this thesis we also show that carefully designed experiments can easily separate most of these electrons from convoy electrons, which are electrons in low lying continuum states of the ions, emerging with the ions from the foil.

Most beam-foil interaction experiments use the setup outlined in the schematic diagram shown in Figure 1. A highly collimated ion beam is passed through a thin foil target. Upstream of the foil the ion energy, charge state and angular spread are set by the experimenter.

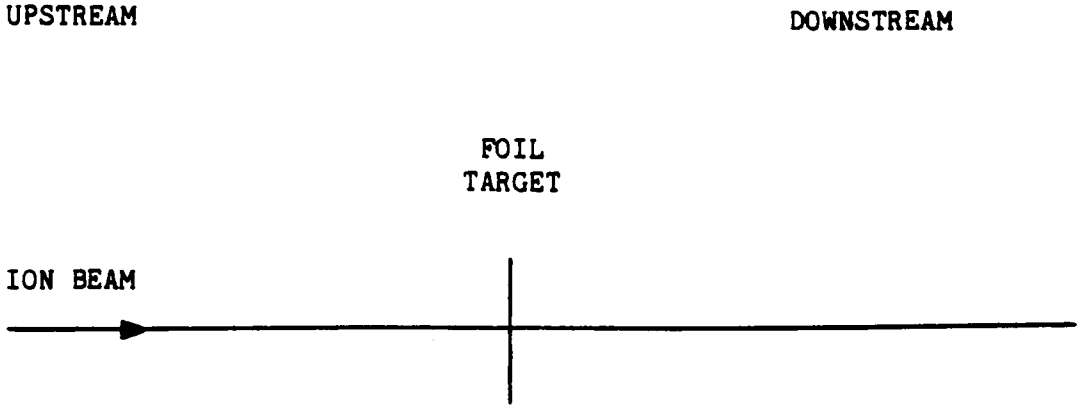

Know:

Charge state

Energy

Angular spread

Measure:

Charge state distribution

Excited state distribution

Free electron energy and angular distributions

Figure 1. The typical setup for beam foil experiment.

Downstream of the foil different experimental techniques are used to measure the emergent ion charge state distribution, the excited state distribution for different charge states, the energy and angular spread of the exiting beam, or the energy and angular distribution of electrons emerging with the ion beam.

It is not necessarily the goal of all beam foil experiments to investigate the ion solid interaction. In many experimental setups the beam foil interaction is a tool for experiments downstream. Stripping foils are routinely used in accelerators to produce high charge state ion beams. The goal of beam foil spectroscopy is to determine the energies and lifetimes of excited electronic states of single ions and atoms. However a central question asked by many experimenters is still: What can the downstream measurements reveal about the fundamental interactions between an ion and a foil?

A foil is normally considered a thin film. Nonetheless it may be divided into several regions (see Figure 2a) along with the surrounding environment.[2] Processes in each region can influence the observations far downstream. Some of the processes that need to be considered are listed in Figure 2b. The foil interior, the last layer, and the region immediately beyond the surface may all influence the emergent ion charge state and excited state distributions and the energy and angular distribution of electrons accompanying the exiting ions.
It is apparent that great care must be exercised in drawing conclusions from what is measured downstream about the fundamental beam foil interactions. Models treating the beam foil interaction as a succession of single ion-atom collisions are tried as a first approximation.

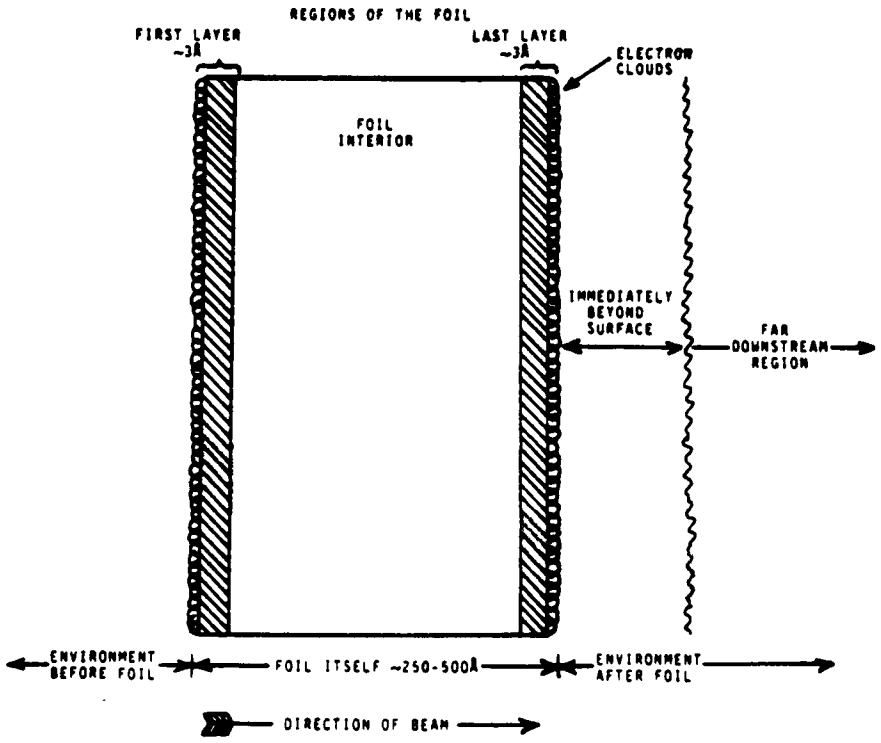

(A) Regions of the foil and vicinty.

Figure 2. The various aspects of a foil.

Source: J. Davidson, W. S. Bickel, Nucl. Instrum. Methods 110, 255 (1973).

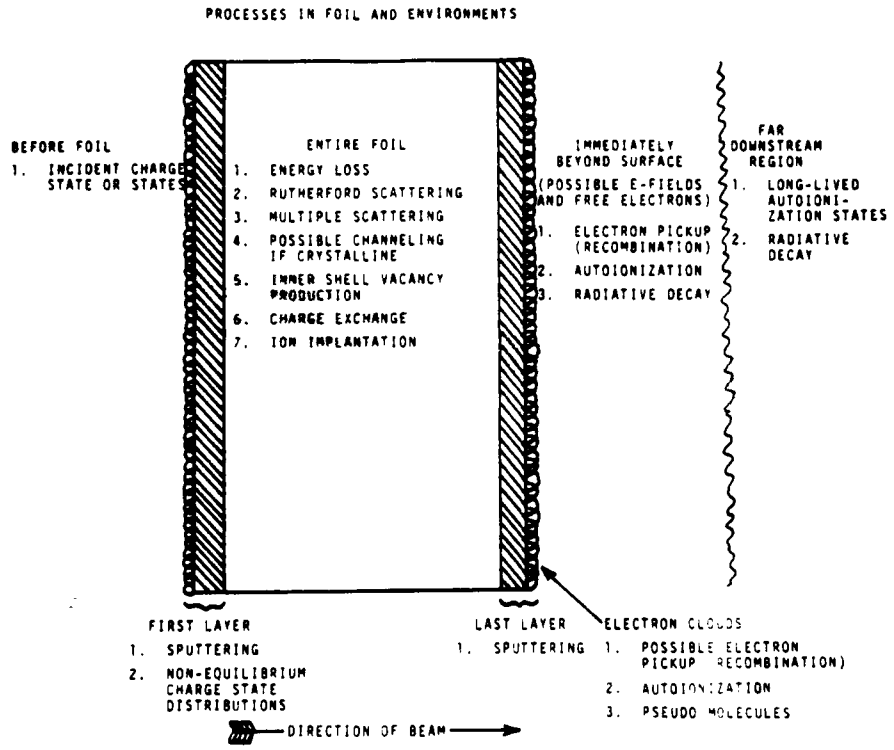

(B) Processes in the foil and its environment which may contribute to the formation of the beam-foil states observed downstream.

Figure 2 (continued)

However the beam foil interaction is much more involved. At present not even the connection between the emergent charge state distribution and the charge state distribution of the ions inside the foil is completely understood.

B. Foil Excited Rydberg States

Central to Niels Bohr's early work in 1913 was the physics of atoms in which an electron is excited to an exceptionally high energy level. Such atoms are commonly referred to as Rydberg atoms and the electrons are said to be in Rydberg states. Using the compiled spectroscopic data of highly excited hydrogen atoms, Bohr laid the ground work for the early quantum mechanics. From the investigations of these excited states he introduced the conceptually important correspondence principle that spanned the gulf between the macroscopic and microscopic universe. (In doing so he allowed some of the old tools of classical mechanics to be utilized in the new realm of atomic physics). To this day, various aspects of Rydberg atoms still intrigue researchers.

One interesting aspect concerning Rydberg atoms is that any atom can be made into one by promoting one of its electrons to a very high energy level.[3] Rydberg atoms typically are enormous in size and some have been detected with diameters on the scale of a hundredth of a millimeter (1×10^5 times the diameter of an atom in the ground state).

In general Rydberg atoms possess the following characteristics:

1. They have long lifetimes (from a thousandth to a full second long)
2. They can be stripped by modest electric fields and can be squeezed into unexpected shapes by magnetic fields.
3. They are hydrogenic in their essential properties

Another rather fascinating point concerning Rydberg states of atoms and ions, especially those of high degeneracy (i.e. those of high orbital angular momentum ℓ) is the role they play in astrophysical and laboratory plasmas, when radiative recombination governs the macroscopic properties of the medium.

This was the motivation during the 60's and 70's for investigating high n states of hydrogen atoms in fast beams. These studies were to investigate the possibility of using "Lorentz-ionized" Rydberg states of hydrogen's heavy isotopes to fuel and heat plasma devices being used for thermonuclear fusion experiments.[4]

After passage through a thin foil target an ion may exit in a Rydberg state. It is currently still an open question of how and where in the foil these highly excited states are formed and how much information about the beam foil interaction can be extracted from the measured excited state distributions.

It is generally accepted that the observed Rydberg states are not formed inside a solid because of screening of the target atoms and the rapid collision frequency.[5] It is safe to assume that the actually observed Rydberg states are created during and after passage of the projectile through the exit surface of the foil target, because the

destruction cross sections for such states in the solid are so large. In a classical picture the diameters of high Rydberg states are much larger than the distances between the centers of adjacent atoms in a solid and therefore these states simply cannot exist deep inside a solid. However, the creation of a particular excited state depends to a certain extent on what sort of atom is reaching the last layer of the foil. Therefore the excited state distribution may still carry information on what occurs in the interior region of a foil.

How are Rydberg states of fast heavy ions formed in or near the last layer of the foil? Are these states formed by Coulomb capture of target electrons from the last layer, similar to electron capture in single ion-atom collisions? This process at large collision velocities $\vec{v}$ may be approximated by the Oppenheimer-Brinkman-Kramers (OBK) formalism. Or are the Rydberg states due to bound-bound excitation of projectile electrons in collisions with last-layer target atoms? For single ion atom collisions first order Born approximation calculations are expected to describe the various excitation probabilities with reasonable accuracy. "Last layer" models for the production of foil excited high Rydberg states usually invoke the above processes.

However, recently Betz et al. have presented data which argue strongly against both last layer OBK type electron capture and bound-bound excitation of projectile electrons as the production mechanisms for the Rydberg state observed downstream of a foil.[5,6]

Passing 127 MeV sulfur and 40-60 MeV oxygen beams through 2-220 $\mu g/cm^2$ carbon foils Betz et al. have measured the number of K x-rays per hydrogen-like ion emitted downstream as a function of target

thickness and target detector distance.[5,6] They assume that foil excited Rydberg states decay via several intermediate states to 2p or 3p states and then give rise to Lyman-α and Lyman-β radiation respectively. They then try to deduce the initial quantum state population $P(n,\ell)$ of the foil excited states which leads via cascading to the observed ratios of Ly-α to Ly-β of 30 to 50. Low ℓ Rydberg states give rise to Ly-α to Ly-β ratios of 3 to 5. They conclude that the observed Ly-α radiation is primarily due to high ℓ Rydberg states, which are not predicted to be populated by the OBK formalism or by the first Born approximation for bound-bound excitation of projectile electrons. They are also not observed when fast ions pass through dilute gas targets.

A hypothetical multi-step model for the formation of Rydberg states of fast ions emerging from solid targets was proposed by Betz et al. As shown in Figure 3, in this model Rydberg states are formed at the surface by the capture of correlated convoy electrons into highly excited states of the ions.[7]

Betz et al. detect foil excited Rydberg states by monitoring the K x-rays emitted after a cascading decay.
They can resolve decays from well defined charge states and can test initial n,ℓ distributions for values of n which are not too large ($2 < n < 120$).

In this thesis we test the initial quantum state population $P(n)$ of highly excited Rydberg states of oxygen ions ($n > 100$) using field ionization techniques, which have been shown to be very efficient tools in the detection and analysis of Rydberg states.[8,9,10,11]

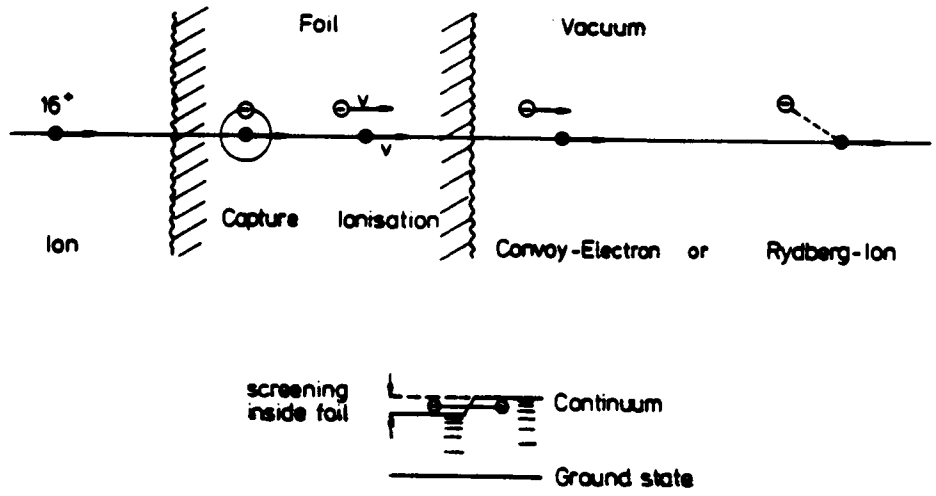

Figure 3. Hypothetical multi-step model for the formation of Rydberg states of fast ions emerging from solid targets.

Source: H. D. Betz, in Lecture Notes in Physics. 213, edited by K. O. Groeneveld, W. Mechbach and I. A. Sellin, (Springer, Berlin, 1984), p. 115.

Field ionization may be described either classically or quantum mechanically. The classical view is based on simple energy arguments. With an electric field F applied along the z-axis the potenial energy of an electron is of the form

$$U(r) = (-1/4\pi\varepsilon_0)(Z_{eff}\, e^2/r) + eFz \qquad (1)$$

Here $e = +1.6x10^{-19}C$ and Z_{eff} is the effective nuclear charge in units of e. This potential energy has a saddle point on the z-axis at $z_{sp} = (Z_{eff}e/4\pi\varepsilon_0F)^{1/2}$ where it has the value $U_{sp} = -2(Z_{eff}\, e/4\pi\varepsilon_0)^{1/2}\, F^{1/2}$ (see Figure 4). According to the classical model, also called the saddle point model, a state is stable or ionizes as to whether the energy E is lower or higher than U_{sp} respectively. Bound states have energies $E < U_{sp}$, while states with energies $E > U_{sp}$ ionize immediately.

In the quantum mechanical picture, ionization occurs by tunneling of the electron through a potential barrier along the z-axis. Tunneling rates increase with the applied field so rapidly that often it is a good approximation to take the rate as zero for $E < U_{sp}$, and infinite for $E > U_{sp}$.

For Rydberg states with high principal quantum number n, experiments show that the classical model characterizes the ionization process well.[12,13,14] If Stark splitting is neglected the value of the electric field which ionizes all excited states with principal

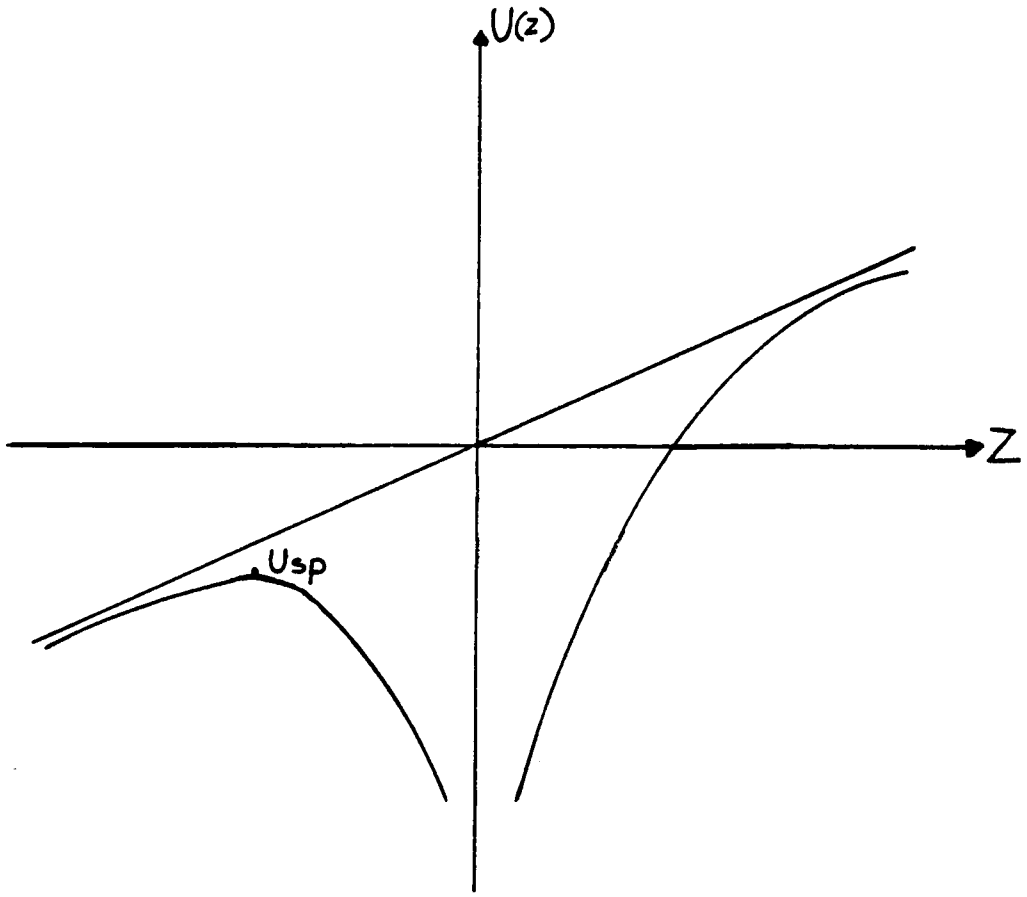

Figure 4. The shape of the saddle point potenial energy of equation (1).

quantum number n' > n (called the critical field value) is given by [15]

$$F_c = 3.12 \times 10^8 \, Z_{eff}^3/n^4 \text{ V/cm} \qquad (2)$$

The Z_{eff}^3/n^4 scaling has been shown to hold, even though the coefficient for the critical field value has been shown to differ from that given in equation 2 for different Stark states. It is this Z_{eff}^3/n^4 scaling which allows us to use field ionization as a probe of the quantum state population distribution P(n) of excited Rydberg states of ions emerging from a foil.

An applied electric field always ionizes all the electrons with principal quantum number $n > n_c$ where $n_c \propto (Z^3/F_c)^{1/4}$. If a foil excited ion beam passes successively through two regions with constant electric fields of different strengths, a particular band of excited states can be examined. This experimental method is used in our work. After emerging from a carbon foil target a beam of (1-2MeV/u) foil excited oxygen ions passes through a region with constant electric field F_1 between a pair of parallel plates called the ionization plates (see Figure 5). It then enters an electrostatic spherical sector electron energy analyzer. The electric field F_2 midway between the analyzer plates is always greater than F_1. The electric field F_1 ionizes all electrons with principal quantum number $n > n_1$, where $n_1 \propto (1/F_1)^{1/4}$ and deflects them away from the entrance of the analyzer. Rydberg states with $n_1 > n > n_2$ ($n_2 \propto (1/F_2)^{1/4}$) are ionized as the ion beam enters the electrostatic electron energy analyzer. Electrons

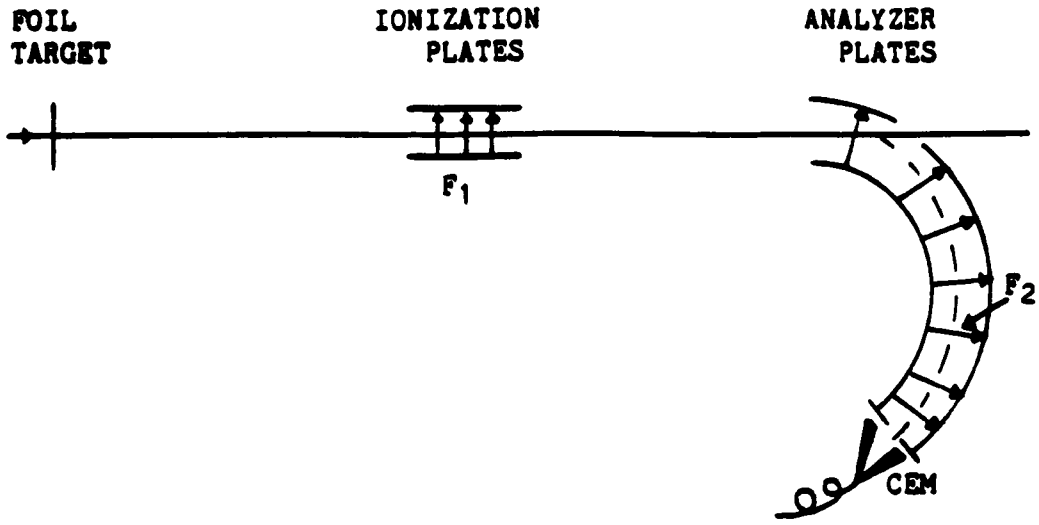

(A) The two electric fields used to ionize the Rydberg states.

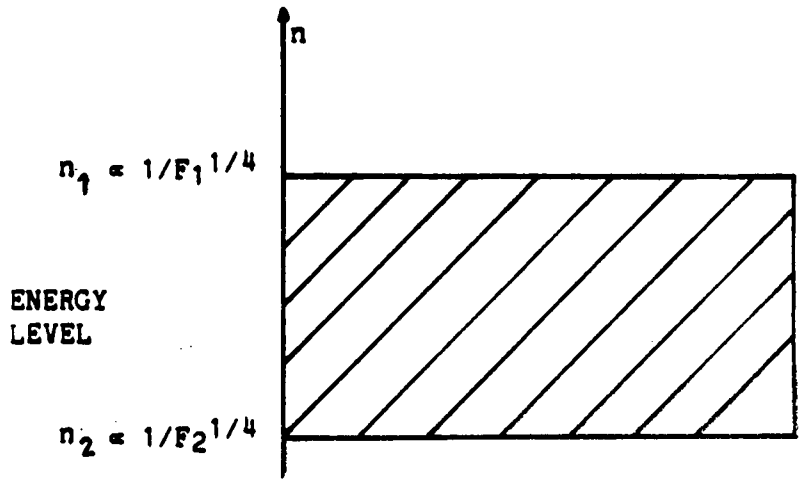

(B) Only electrons from the states $n_1 > n > n_2$ are detected.

Figure 5. Experimental setup to examine a particular band of foil excited Rydberg states.

ionized at the entrance of this analyzer have velocities near the beam velocity and are energy analyzed by the analyzer and detected in a channel electron multipiler (CEM). The number of electrons detected is proportional to $\int_{n_2}^{n_1} P(n)dn$, where P(n) is the quantum state population distribution of the foil excited Rydberg states.

For 0.75 MeV protons traversing carbon foils, it has been reported by Vager et al. that an electric field perpendicular to the beam direction is much more effective in field ionization of Rydberg states than a field along the beam direction.[16] This is taken as an indication of strong alignment in the excitation, suggesting a highly oblate electron density in the Rydberg states with respect to the beam direction. Checking for indications of initial nonstatistical sublevel population for oxygen ions traversing carbon targets, we rotated the ionization plates so that the direction of F_1 is either perpendicular or parallel to the beam direction. With F_1 parallel to the beam direction a pair of deflection plates is inserted between the ionization plates and the analyzer so that a weak electric field transverse to the beam direction can deflect electrons ionized by F_1 away from the entrance of the analyzer.

While making measurements to characterize the quantum state population P(n), oscillations of the Rydberg electron yield as a function of the ionization field F_1 were observed for both transverse and longitudinal field directions. We will show that these oscillations may be ascribed to coherent excitation of high Rydberg states by the beam-foil interaction.

C. Convoy Electrons

When fast ions tranverse a solid or gaseous target, a sharp cusplike peak is observed in the energy spectrum of electrons emitted in the forward direction. The electron velocity $\vec{v}_e$ at the tip of the cusp equals the velocity of the emerging ion $\vec{v}$. For solid targets, electrons with velocities $\vec{v}_e \cong \vec{v}$ are called convoy electrons.

Convoy electron energy spectra are traditionaly measured by placing a foil in the entrance focus of an electron energy analyzer and recording the energy distribution of electrons emitted into a cone of half angle Θ_0 about the forward direction as a function of the analyzer field and the ion beam current. A typical setup is displayed in Figure 6. Electrons emitted at the entrance focus are refocused at the exit focus of the analyzer. An aperture in the exit focus determines the energy resolution $\Delta E/E$ of the analyzer while a second aperture sets the acceptance angle Θ_0.

The velocity spectra of convoy electrons measured with such a setup display nearly symmetric cusps peaking at beam velocity.[16] For equilibrium thickness foils the shape and width of these cusps are nearly independent of the projectile speed, projectile nuclear charge Z, and target nuclear charge Z_t. Yet the integrated cusp yields display a common velocity dependence, and a velocity-independent Z dependence given by $E^{-2.25}\ Z^{2.75}$,and depend only weakly on the target material.[16] An interesting but puzzling fact in the study of convoy electron cusps is the independence of the convoy yield per exiting ion on the charge state of the ion for heavy projectiles and equilibrium thickness

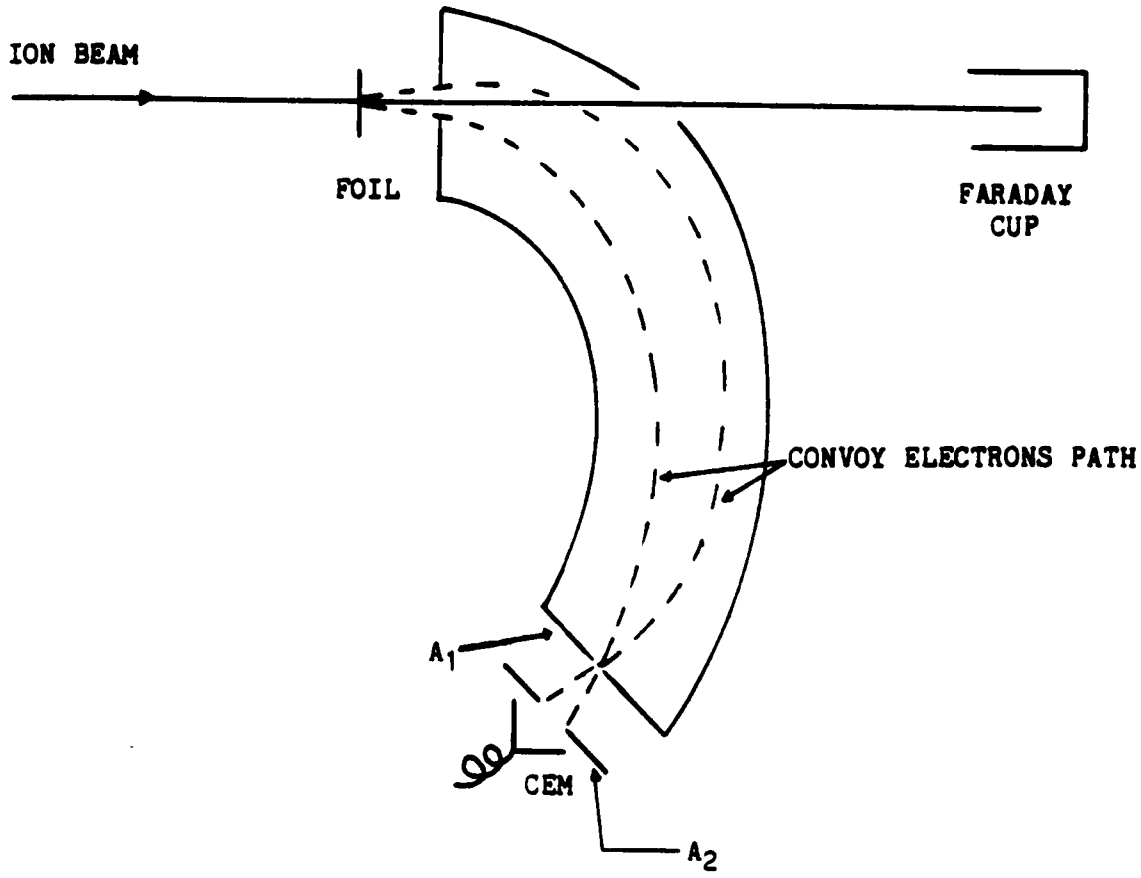

Figure 6. A typical setup to measure electron energy distributions. The target is placed in the entrance focus of the analyzer. An aperture A_1 in the exit focus determines the energy resolution while a second aperture A_2 limits the acceptance angle θ_o of the analyzer.

targets. This in spite of the observed strong Z dependence.

A prime question under examination today is whether the same processes responsible for the production of cusp electrons in a gaseous target are at work in a solid target. Cusp spectra from gas targets are recorded using a setup as shown in Figure 6 with the exception that a gas cell is placed (and centered) at the entrance focus of the analyzer. For gas targets two different production mechanisms for cusp electrons, electron capture to the continuum (ECC) and electron loss to the continuum (ELC), have been identified.[17]

The ECC process involves a violent collision and a large momentum transfer to a target electron. An electron is transferred from a bound state of the target into a low lying continuum state of the projectile. The ELC process involves a soft collision and a small momentum transfer. Here, a previously bound projectile electron is transfered to a continuum state of low momentum with respect to the projectile nucleus.

The shape of the ECC cusp is asymmetric with a sharp drop off on the high velocity side and a width scaling roughly as the ion velocity v. The ECC cusp is generally narrower, nearly symmetric and has a width nearly independent of velocity.

It has been speculated that ECC processes near the exit surface of a solid target are responsible for the production of convoy electrons. However, when comparing convoy cusps and ECC cusps, measured with heavy ion projectiles, distinct differences in the cusp shapes are observed. The symmetrical shape of the convoy cusp argues against a last layer ECC production mechanism for convoy electrons. It has been noted

though that the shape and width of convoy electron cusps are very similar to those of the ELC cusps measured for heavy projectiles and gas targets.[17]

Recently strong target thickness dependence of the convoy electron yield, normalized to the beam current, has been demonstrated for non-equilibrium thickness foil targets. This target thickness dependence suggests that convoy electrons escape from regions deep inside the solid target. The observed convoy yields increase with target thickness over a distance up to about ten times the length of the mean free path for free electron scattering. A convoy electron production mechanism has been proposed which is based on a bound state electron capture event inside the solid target followed immediately by electron loss. This model can explain the apparent increase in the mean free path of convoy electrons over free electrons by taking Coulomb focusing into account.[18]

Recently, Yamazaki and Oda, using hydrogen projectiles on carbon foils, measured a weak charge state dependence of the convoy yield. These investigators propose another convoy electron production mechanism, free electron transfer to the continuum (FETC).[19] They observe that even though the shape of the background changes as a function of target thickness, the ratio of the convoy peak intensity to the background intensity does not. They suggest that a final state interaction between projectile ion and the background electrons produces the observed convoy electrons.

D. Present Dispute

In a recent Physical Review Letter, using H^+, He^+ and Ne^+ projectiles on carbon foils, Vager et al. suggest that some of the puzzles surrounding convoy electron production might be resolved if researchers realized that a significant fraction of the electrons measured in the convoy electron cusp are not really convoys at all.[20] It is well known that Rydberg states have long radiative lifetimes, but that they can be ionized by relatively weak electric fields. Vager et al. present data implying that highly excited Rydberg states, field ionized inside the electron energy analyzer used to measure the energy spectra of convoy electrons, are responsible for a large fraction of the electrons measured in a traditional convoy cusp. Many investigators strongly disagree with this suggestion.[21,22,23] Are convoys electrons really Rydberg electrons ionized by the analyzer field? This thesis presents results demonstrating that highly excited Rydberg states, field ionized inside our electron analyzer, do not significantly contribute to the convoy electron cusp spectra measured for fast oxygen ions on carbon foils.

Chapter II

APPARATUS AND EXPERIMENTAL METHOD

A. Beam Line Sections

The 18 MeV O^{+3} and 32 MeV O^{+5} ions used in our experiments were provided by the ORNL EN Tandem accelerator. After being momentum analyzed by a set of analyzing magnets, the ions entered the beam line containing the experimental setup as shown in Figure 7. A vacuum of 5×10^{-8} torr was maintained upstream of this beam line section.

A magnetic quadrupole doublet lens QD (see Figure 7) focussed the beam onto the front of a collimator system, A1. The collimator system consisted of a set of two circular apertures with diameters 2mm and .71mm, respectively, separated by a 5mm distance. The upstream 2mm aperture was held at ground potential, while the downstream .71mm aperture was used to monitor beam current. This entire collimator system could be moved in or out of the beam's path.

A second collimator A_2 was located 1.03m downstream. It consists of a metal plate, with three aperture holes, which is mounted on a x-y manipulator stage for easy alignment. Hole diameters were .35mm, .71mm and 6.35mm. The largest hole was used for alignment purposes. Collimation with an angular spread of 0.03 degree (half angle) was possible.

The section of the beam line containing the collimator system and the experimental chamber was maintained under high vacuum by two Varian (NRC) oil diffusion pumps, DP1 and DP2 (see Figure 7). A vacuum of

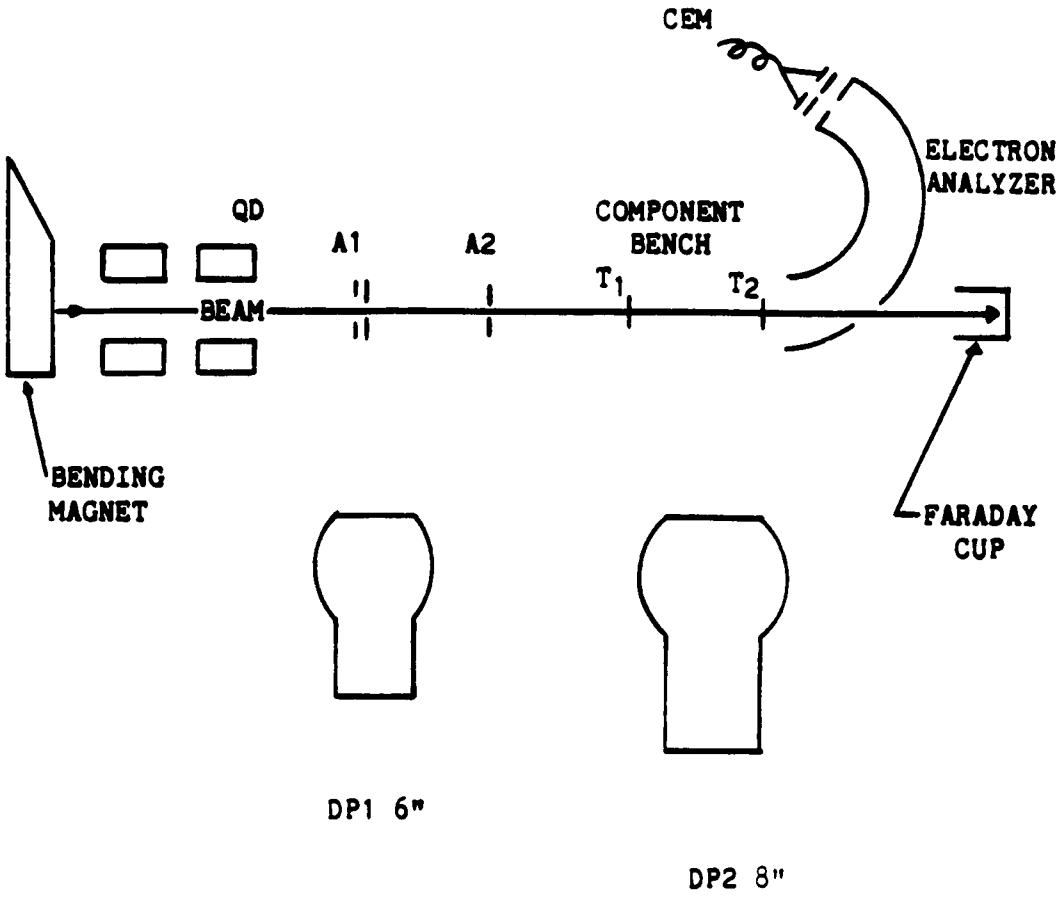

Figure 7. The various parts of the beam line. Ions emerging from a bending magnet are focused by a magnetic quadropole (QD) onto the collimator systems (A_1,A_2) and then encounter the experimental package consisting of component bench, electron analyzer and CEM. The beam terminates in a Faraday cup. Vacuum for the beam line is maintained by diffusion pumps DP1 and DP2.

better than 1 x 10^{-7} torr was maintained throughout the beamline section. A residual gas analyzer monitored partial pressures and checked for any impurities present in the chamber.

B. Experimental Package

The experimental chamber held a component bench and a electrostatic spherical sector electron energy analyzer. The component bench is designed to serve two purposes. First it must provide a flat level supporting surface for targets and different sets of electrostatic ionization and deflection plates with a consistent internal alignment. Second, it must allow alignment of this entire setup with the ion beam.

A detailed drawing of the component bench is shown in Figure 8. The bench is composed of two flat thin aluminum plates, a top plate A and a bottom plate B. Both plates are connected via a tripod arrangement of three threaded studs. Two foil target holders and two sets of electric field plates can be mounted on plate A. As seen in the figure, the foil holders are mounted in positions 5 and 8 while the ionization plates are mounted in position 6 and the deflection plates in position 7.

Because the component bench can be aligned precisely, one of the foil targets can be accurately placed at the entrance focus of the electron energy analyzer. A second foil target can placed 20 cm upstream of this focus.

This accurate placement is essential in the direct comparison of electron spectra from the two positions. Measurements were made using

Figure 8. Component Bench Assembly

1 - Foil target holder (out of focus)

2 - Ionization plates

3 - Deflection plates

4 - Foil target holder (in focus)

5 - Mounting hole for target holder (out of focus)

6 - Mounting hole for Ionization plates

7 - Mounting hole for Deflection plates

8 - Mounting hole for foil target (in focus)

9 - Top plate A

10 - Machined corner slot

11 - Machined rounded locknuts

12 - Threaded stud

13 - Support bars

14 - Bottom plate B

15 - Metal tracks

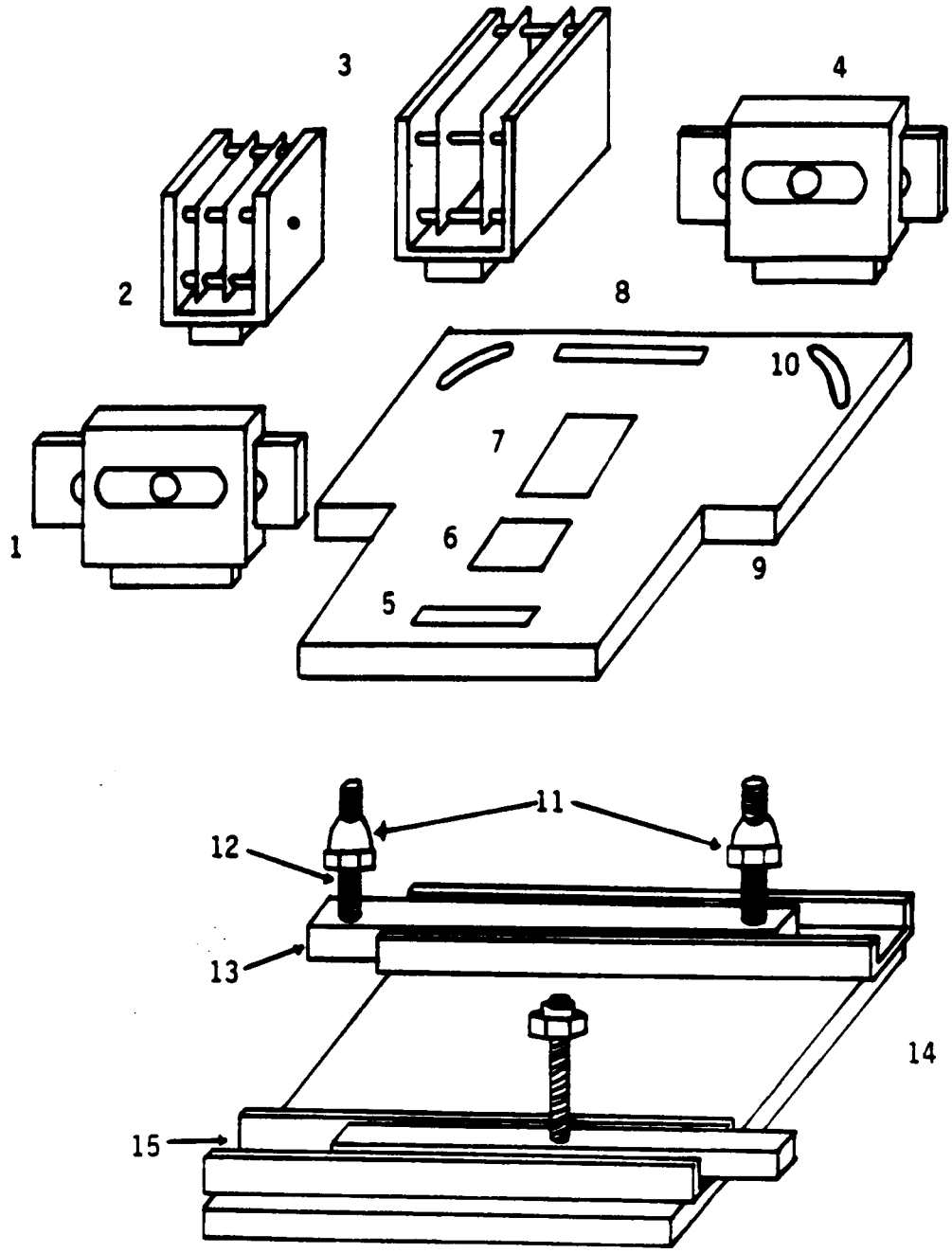

Figure 8. Component Bench Assembly

15μg/cm² and 30μg/cm² carbon foils. Commercially purchased carbon foil material was floated onto target ladders. Each ladder has three holes, two were covered by foil material while the third remained open for alignment purposes and background measurements (see Figure 9). The ladder fits securely into a machined groove, recessed in the surface of the target holder, for smooth reproducible motion. At any given time only one target was positioned in the path of the beam.

The electric field plates called the ionization plates are shown in the lower half Figure 9. The plates are supported and shielded by a housing. The corners of the housings are counterbored and holes are drilled into each corner of the plates. Four long nonconducting rods pass through these holes and lock into the corners of the housing. Spacers, fitting over the rods, maintain the correct distance D between the plates and isolate the plates from the grounded housing.

The ionization plates can be rotated to produce a field longitudinal or transverse to the beams direction. A 2mm diameter hole is drilled through the middle of the ionization plates and the housing to allow passage of the beam when the plates produce an electric field along the beam direction. Voltage to the plates is supplied, via vacuum feed throughs, by a power supply. The second set of field plates, called the deflection plates, are constructed in a similar fashion.

All components on the component bench interlock with the bench via tabs fitting into machined slots with a tolerance of ± 0.05mm. In this way the internal alignment of the components was preserved even though they could be exchanged in the course of the experiment.

Figure 9. Foil Targets and Electrostatic Plates

Description	Dimensions
1 - Carbon Foils	15 and 30 $\mu g/cm^2$
2 - Foil Ladder	50mm x 27mm x 3mm
3 - Ladder Holder	48mm x 10mm x 50mm
4 - Locking Tab	15mm x 16mm x 4mm
5 - Ionization Plate Housing	28mm x 44mm x 46mm
6 - Corner Counterbored Hole	3mm in diam. 2mm deep
7 - Spacers (left and right sides)	7mm in diam. 8mm long
8 - Al_2O_3 Rod	2.5mm in diam. 25mm long
9 - Separation Distance Spacers	
a) Ionization Plates	4mm
b) Deflection Plates	5mm
10 - Ionization Plates	38mm x 38mm x 1mm
11 - Removable Housing Wall	56mm x 48mm x 3mm
12 - Locking Tab	50mm x 15mm x 4mm
13 - Deflection Plate Housing	56mm x 44mm x 46mm
14 - Deflection Plates	50mm x 38mm x 1mm
15 - Locking Tab	50mm x 15mm x 4mm
16 - Removable Case Wall	56mm x 46mm x 3mm

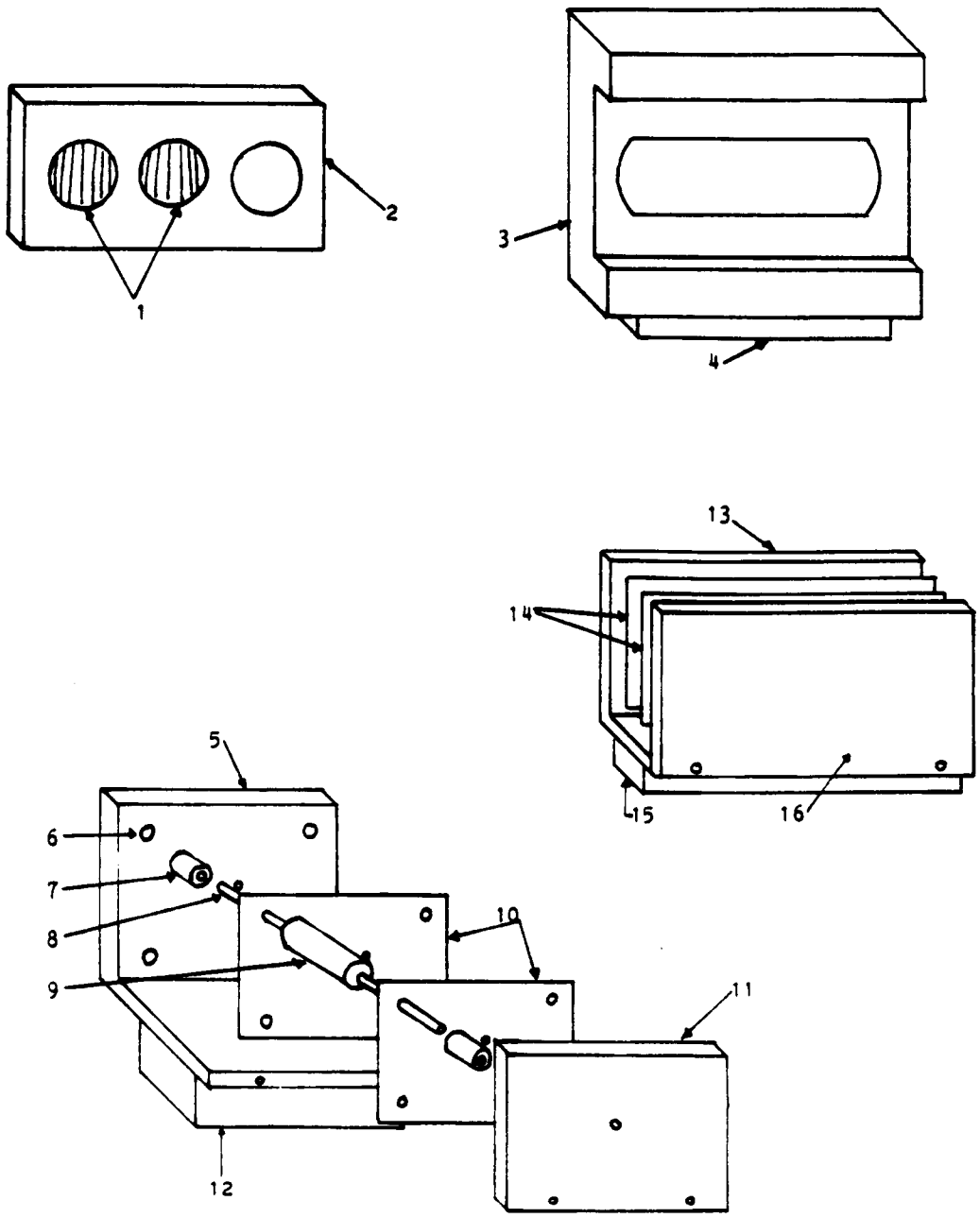

Figure 9. Foil targets and electrostatic plates.

Successful alignment of the top plate A, to the beam and the electron analyzer is possible because of the special design of the bottom plate B which was bolted to the inside of the experimental chamber. As shown in Figure 8 two metal tracks are fastened at each end of plate B. Each track allows for the easy movement of two bars which hold the threaded studs. As indicated in the figure the position of the bars determines the horizontal alignment of the top plate A.

Vertical alignment for the top plate is achieved by securely tightening specially machined rounded locknuts at the appropriate height on the threaded studs. Plate A then rests on these locknuts and a second set of locknuts locks it into place from above. The tripod configuration of the studs provides a high degree of rotational freedom for the top plate, in the horizontal plane. A single stud on the forward track serves as a pivot point. Rounded locknuts on the two rear studs fit into machined slots beneath each corner of the top plate and allow oscillation-free rotation about the pivot point.

The same mounting scheme that is used to align the component bench is also utilized to align the electron energy analyzer. All parts of the experimental setup are aligned with a telescope upstream, viewing the beam line section through the bending magnet.

A light source is located at the downstream end of the experimental chamber, where a Faraday cup is normally positioned. The telescope defines an optical axis with which the electron analyzer, the component bench and collimation system, are aligned.

A spherical sector electrostatic electron energy analyzer is used in our experiment to measure the energy distribution of field ionized Rydberg electrons and convoy electrons in the laboratory frame. Figure 10 shows the main features of such an analyzer.[24] In general an analyzer is asked to accept a beam of charged particles which is diverging in two dimensions at the entrance slit. Angles α in the plane of the analyzer and β in the perpendicular plane are measured from the direction of the central ray. The limiting values of these angles are $\pm\alpha_m$ and $\pm\beta_m$. For the central ray the ratio of the analyzer potential V_p to the energy E_0 passed by the analyzer is a constant depending on the geometry. The analyzer constant is defined as $C = eV_p/E_0$.

For a spherical sector analyzer with inner radius a and outer radius b the field is radial and equal to

$$F = (V_p/r^2)ab/(b-a) \qquad (3)$$

It follows that the relation between the energy E_0 of the central ray and the analyzer potential is such that the analyzer constant is

$$C = (b/a)-(a/b) \qquad (4)$$

Provided the central ray has an initial value of r determined by

$$r_0 = \bar{r} = (1/2)(a+b) \qquad (5)$$

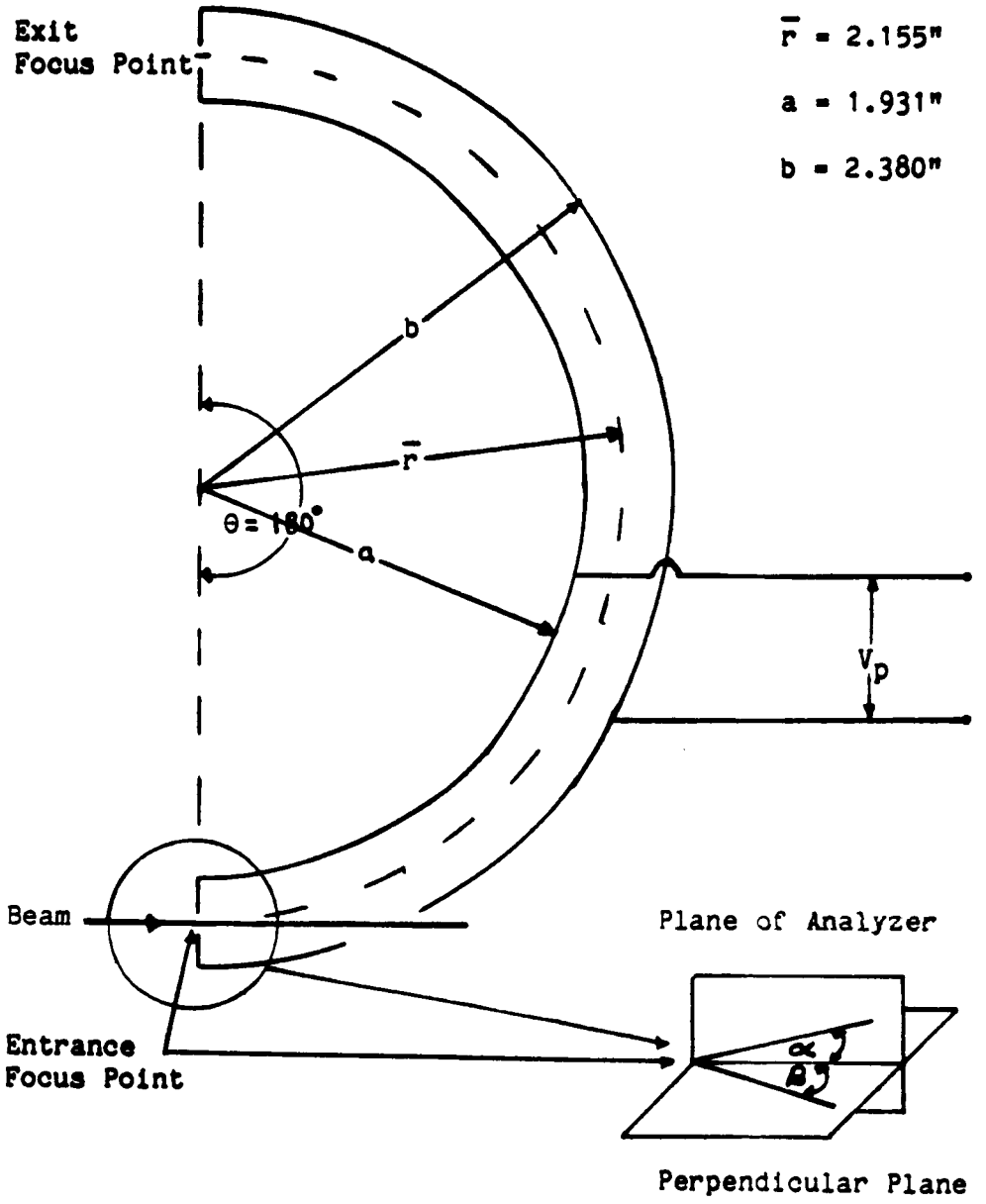

Figure 10. The elements of a 180° sherical sector electrostatic analyzer with its focusing parameters.

so that it enters midway between the spherical plates. The differential equation of the path of a charged particle entering at an arbitrary r_0 is

$$d^2U/d\theta^2 + U = \bar{r}E_0/r_0E\cos^2\alpha \qquad (6)$$

where $U = r_0/r$. Because the spherical symmetry, the analyzer provides perfect focussing for the angle β. The solution of equation 6 is

$$r_0/r = (\bar{r}E_0/r_0E\cos^2\alpha)(1-\cos\theta)+\cos\theta - \tan\alpha\sin\theta \qquad (7)$$

Expanding the factors containing α, we find all powers from the first present. Although, at the angle $\theta = 180°$, the last term will vanish and with it the only first power of α, so for that angle we have first order focussing. Choosing that value of θ and expanding equation 5 to second order in α yields

$$r_0/r_{180} = (2E_0\bar{r}/Er_0)\ (1+\alpha^2) - 1 \qquad (8)$$

For our analyzer $\theta = 160°$ and therefore the analyzer is no longer first order focusing in α. However the deviation from first order focussing in the plane of the analyzer is small.

The combined distance of the entrance and exit focus from the edges of the analyzer plates for our $\theta = 160°$ analyzer is 1.9cm, which allows easy positioning of the foil target at the entrance focus. Figure 11 shows this analyzer in conjunction with the

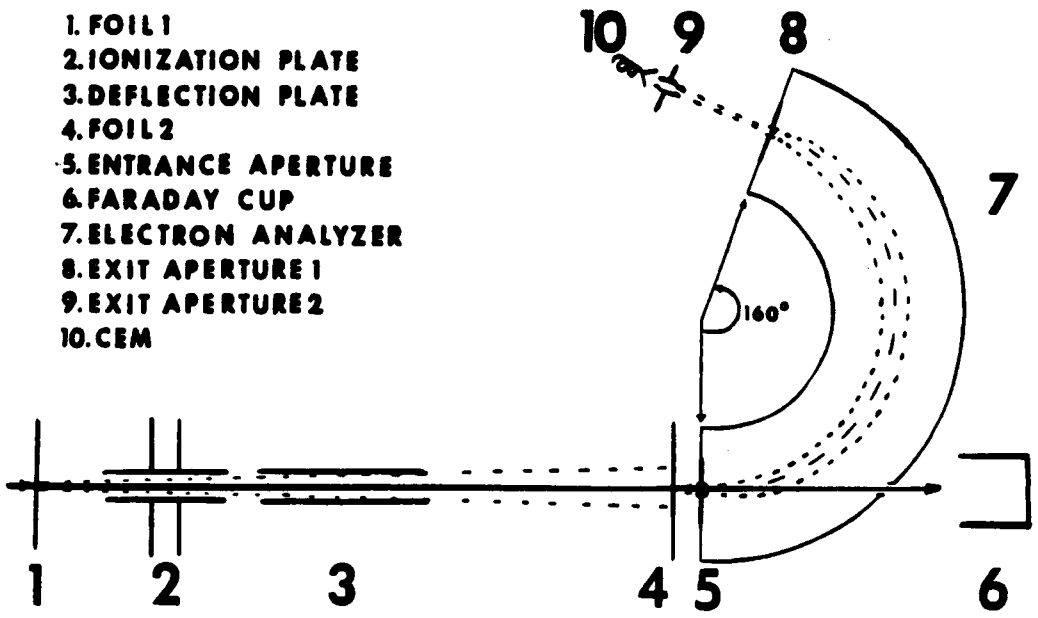

Figure 11. The 160° spherical sector analyzer and experimental setup.

package. For a $\Theta = 180°$ analyzer both entrance and exit foci lie in the plane of the plate boundaries and target positioning at the entrance focus becomes important (Figure 10).

Our analyzer is operated with $V = 0$ at $r = r$, using a programmable DC power supply with floating output and a voltage divider. The energy resolution of the analyzer was set by a 1mm diameter aperture at exit the focus and the < 1mm beam spot size on target at the entrance focus. The energy resolution was 0.9% FWHM. The transmission function of the analyzer operated in this fashion is expected to be nearly triangular. This has been verified in earlier experiments.[25] A second 2mm diameter aperture located 3.8cm away from the exit focus sets the angular acceptance of the analyzer for electrons originating at the entrance focus. It accepts all electrons emitted from the entrance focus into a cone of half angle $\Theta_0 = 1.5°$. The acceptance angle for electrons originating from some position other than the entrance focus will in general, not be determined by this second aperture but by the size of the entrance hole into the analyzer. The acceptance angle can be severely reduced if the electrons originate any appreciable distance away from the entrance focus.

The electrons are detected by a channel electron multiplier (CEM) located behind the angle defining aperture. The CEM is housed in an aluminum box which shields it against stray electrons. A 4000 volt potenial is applied across the CEM, while the CEM cone is biased at -200 volts to suppress spurious background secondary electrons.

External stray magnetic fields can influence the trajectories of electrons to be energy analyzed. Particularly sensitive to such fields

are the electrons emerging from the out of focus target. To reduce stray magnetic fields, three mutual perpendicular sets of Helmholtz coils were installed centered about the entire experimental chamber. These sets of coils allowed us to reduce the stray magnetic fields inside the chamber to ≤18mG.

The field component perpendicular to the beam direction has the strongest influence on trajectories of the electrons originating from the out of focus target. It is perpendicular to the electron velocity. Electrons can be deflected 3.2mm by a field of 140mG and can therefore be prevented from entering or exiting the analyzer. We observed that the transmission efficiency of our analyzer depends strongly on how well external magnetic fields are nulled. Magnetic fields can also change the effective analyzer constant.

C. Electronics and Data Acquisition

Convoy and field ionized Rydberg electron energy spectra are measured by stepping the voltage V_p across the analyzer plates from V_{min} to V_{max} (see Figure 12). For each voltage setting only electrons with energy $E = eV_p/C$ are transmitted and detected. The number of electrons detected is recorded as a function of V_p for a chosen amount of beam charge collected in the Faraday cup, which is proportional to the a chosen number of projectiles entering the cup.

A multichannel analyzer (MCA) stores the number of electrons detected with $E = E_x$ in channel x. The analyzer voltage is $V_p = V_x = CE_x/e$. A digital output makes the channel number available to external electronics. After a preset amount of charge has been collected in a

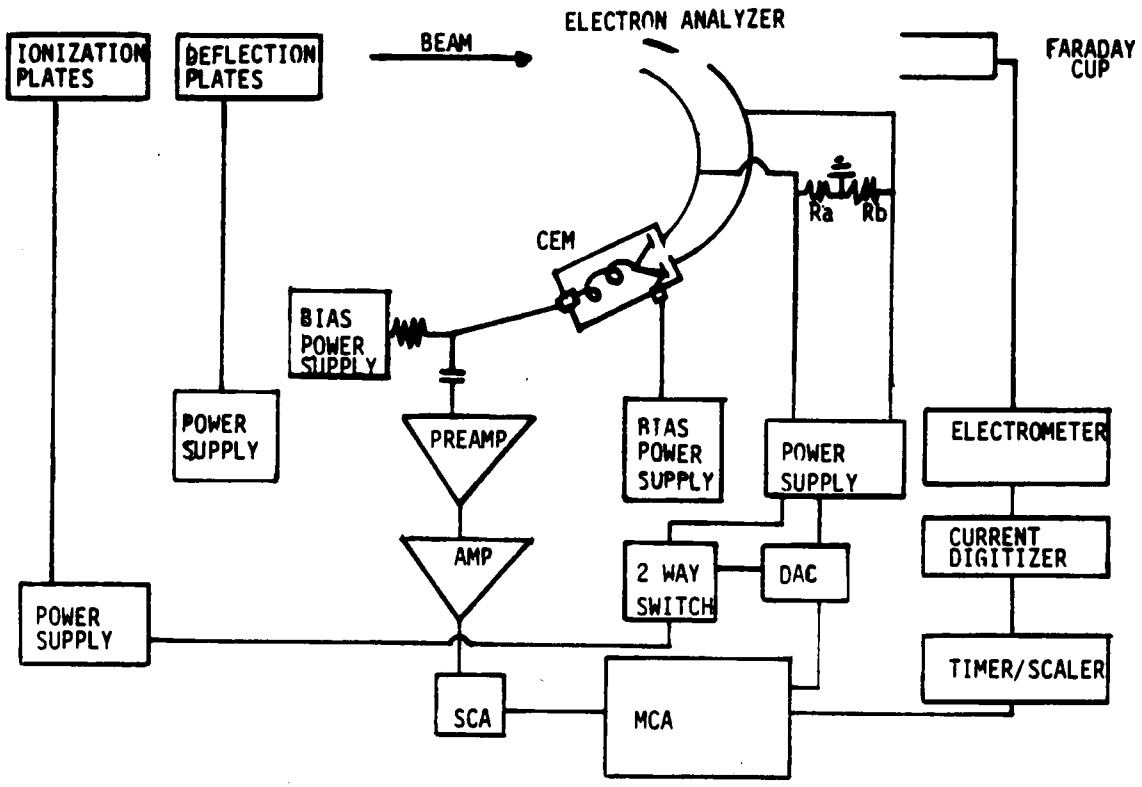

Figure 12. Block diagram of electronics.

Faraday cup the MCA receives an external signal to step to the next channel. The new channel number x+1 appears at the digital output. This output serves as an input to a digital to analog converter (DAC). The analog output of the DAC is proportional to the channel number and is used to program the power supply for V_p. As the channel number is increased by 1, V_p is increased by ΔV to $V_x+\Delta V$, and electrons with energy $E_x+\Delta E$ are tansmitted and detected. Their number per preset amount of projectile charge is stored in channel x+1. After a complete spectrum has been aquired the data are stored on magnetic disk.

For every 10^{-10} Coulombs collected in the Faraday cup a current integrator outputs one pulse. The current integrator pulses are fed into a scaler, which outputs the channel advance signal to the MCA after it has received a preset number of pulses. All counters are gated off for ~ 1μs during channel advance. Since the cone of the CEM is biased to -200 volts, the output pulses occur at positive high voltage and capacitve coupling is used to feed them into a preamplifier. The output of the preamplifier is fed into an amplifier/ single channel analyzer, which for every electron detected sends a pulse to the MCA. While electron energy spectra are measured by stepping the analyzer voltage, the population distribution of foil excited Rydberg states can be measured by fixing the analyzer voltage so that only electrons with velocity $\vec{v}_e = \vec{v}$ are tansmitted and detected. The voltage across the ionization plate is then stepped from 0 to 100 volts using the same electronic setup as described above, except that the DAC output is switched to program a different power supply.

D. Experimental Procedure

In the course of our experiment the following measurements are made:

A) The electron energy distribution is measured for oxygen ions traversing thin carbon targets placed either in the focus or 20cm out of focus of the electrostatic electron energy analyzer. The electrons detected are either convoy electrons coming from the foil or field ionized Rydberg electrons ionized as the beam enters the analyzer. These measurements are made to determine changes in cusp shape and yield as a function of foil position and to set an upper limit to the fraction of field ionized Rydberg electrons in a traditionally measured convoy electron cusp. The measurements are made with 3 different diameter entrance apertures (1.5mm, 3.0mm, 6.25mm) to the analyzer. Special care had to be taken to insure that the 20cm path from the out of focus target to the entrance focus of the electrostatic analyzer was free of stray electric and magnetic fields.

Ionization and deflection plates were grounded and the Helmholz coils were used to null stray magnetic fields. The best Helmholz coil currents were determined by maximizing the cusp yield without distorting the cusp shape.

B) The electron energy distributions are measured for a foil target placed 20cm out of focus of the analyzer as a function of an electric field applied perpendicular to the beam direction between the ionization plates. A voltage between 2 and 50 volts is applied across the ionization plates resulting in a field between 5 V/cm and 125 V/cm. A

deflection field E = 50 V/cm perpendicular to the beam direction is applied to prevent electrons ionized between the ionization plates from entering the analyzer. These measurements are made to determine accurately the fraction of field ionized Rydberg electrons in a traditionally measured convoy electron cusp.

C) The yield of electrons of a given energy is measured as a function of an ionization field, applied either parallel of perpendicular to the beam direction. The voltage across the ionization plates is stepped from 0 volts to 100 volts in 225 steps for a plate seperation 4mm and from 0 to 200 volts for 12mm. The analyzer field is set to analyze electrons with velocity v, $v \pm 0.75\Delta v$, and $v \pm \Delta v$ where v is the beam velocity and Δv is the half width at half maximum of the measured cusp. These measurements are made to determine the quantum state population P(n) of foil excited Rydberg states and to check for signs of alignment in the excitation.

To perform these measurements various components of the experimental package had to be frequently exchanged. This required that the experimental chamber be opened many times during the course of the experiment. Great care was taken to preserve a clean environment inside the chamber. During pump down of the chamber equal caution had to be exercised since the foil targets were particularly susceptible to damage at this time.

CHAPTER III

DATA ANALYSIS AND RESULTS

As stated in chapter one, the predominant goal of this thesis is to demonstrate that traditionally measured convoy electron spectra are not severely contaminated by Rydberg electrons ionized in the field of the electron energy analyzer. The second objective is to determine the initial quantum state population P(n) of foil excited high Rydberg states of oxygen ions. The third objective is to check for signs of an initial nonstatistical sublevel population for foil excited Rydberg states.

A. Determination of Relative Electron Yields

Total electron yields are extracted from the electron energy distributions for oxygen ions traversing carbon foils placed both in and 20cm out of the entrance focus of the electron energy analyzer. Here we define the electron yield Y as

$$Y = \sum_j N(Ej)\Delta Ej/Ej * 1/QS \qquad (8)$$

N(Ej) is the number of electrons counted in the jth channel, Ej the specific energy of these electrons, ΔEj is the difference in electron energy for electrons counted in adjacent channels, Q is the charge collected in the faraday cup during one channel of data collection (given in nanocoulombs) while S represents the number of scans taken.

For heavy ion projectiles, the shape of the convoy electron cusp for an in focus target is nearly independent of the projectile nuclear

charge, the projectile speed, and the target as outlined in chapter I. The full width at half maximum Γ of the longitudinal velocity distribution of convoy electrons emerging from a solid target in the forward direction is approximately $\Gamma = 0.25$ au. To determine the total electron yield we therefore integrate our electron spectra over an energy interval $E \pm \Delta E$ corresponding to the velocity interval $v \pm \Delta v$, where where v is the beam velocity and $v = 0.25$ au. In other words, we extend our summation over a velocity interval equal to twice the FWHM of the convoy electron velocity distribution for an in focus target, centered at the tip of the cusp.

B. Estimation of Quantum State Population P(n)

The ratio of the total electron yield measured with an in focus target to the yield measured with an out of focus target is 21 to 1. Typical electron cusps, which were used to determine this ratio are shown in Figure 13. Part A shows the cusp measured with an in focus target while part B shows the cusp measured with the target, positioned 20cm upstream from the entrance focus of the analyzer. For both cusps the yields are normalized to the beam current. All convoy electrons emerging from the in focus foil target into a cone of half angle $\theta_0 = 1.5°$ are accepted by the analyzer and energy analyzed. However for convoy electrons emerging from the out of focus target the acceptance angle is drastically reduced.

The angle is determined by the diameter of the entrance aperture of the analyzer and for a 2mm diameter aperture is $\theta_0 \approx 0.3°$. Part C of Figure 13 shows an overlay of the two cusps on the same scale. The

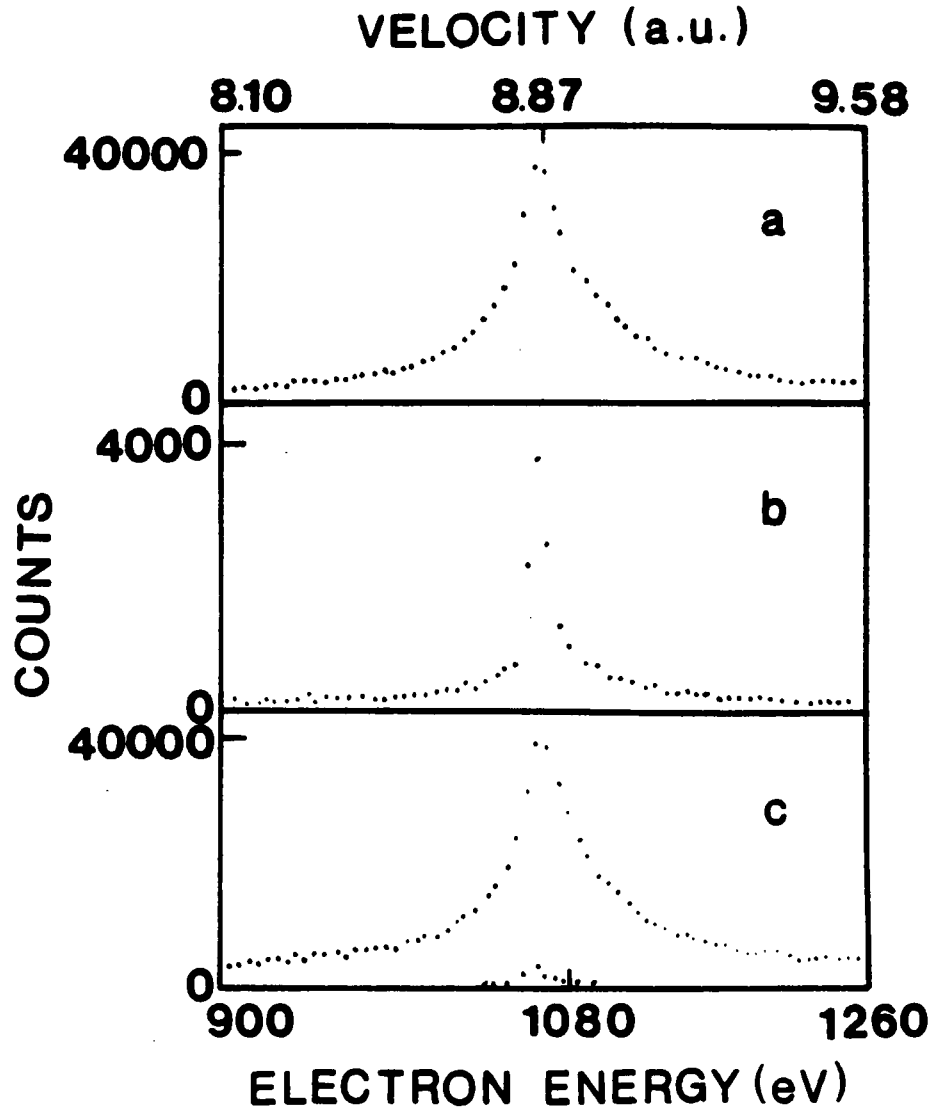

Figure 13. Energy distribution for electrons originating at a) the in focus target and b) the out of focus target. In c) both distributions are overlayed on the same scale.

21 to 1 ratio of the yields agrees roughly with the ratio expected from the change of effective acceptance angle, assuming that the number of foil excited Rydberg states and convoy electrons produced in a foil target is independent of the target position.

The analyzer field in our experiments ionized Rydberg states of oxygen ions with principal quantum number $n \gtrsim 100$. Such states have a very long lifetime against radiative decay. A 32 MeV oxygen ion travels 20cm in about 10 nanoseconds. Thus if no electric fields are present in the region between analyzer and target, then due to the very long lifetimes of the high Rydberg states and very short flight time from a target to the analyzer the number of highly excited ions entering the analyzer does not depend on target position. The yield of Rydberg electrons ionized by the analyzers field (~450V/cm) is therefore independent of target position. However because of the reduced acceptance angle of the analyzer for an out of focus target the measured convoy electron yield dependends strongly on the target position. The fraction of field ionized Rydberg electrons in the convoy cusp will be much greater for the out of focus target. Even if one assumes that this fraction is equal to 1, i.e. that all convoys are lost and only field ionized Rydberg electrons contribute to the yield from the out of focus target, then the contribution of these field ionized Rydberg electrons to the total electron yield measured for an in focus target can not be larger than 1/21 or 4.7%.

This places an upper limit on the fraction of field ionized Rydberg electrons contaminating a convoy cusp measured in the

traditional way, by placing the target in the entrance focus of an electron analyzer.

To determine this fraction more precisely, additional measurements are made with the out of focus target. A weak electric field F_I is applied perpendicular to the beam by applying a voltage across the ionization plates. This field deflects convoy electrons originating from the target and prevents them from entering the electron energy analyzer. Electron energy distributions are measured as a function of this ionization field and are plotted in Figure 14. The integrated yield of electrons transmitted through the analyzer is measured as a function of the field F_I, and shown in Figure 15. For fields between 0 and -50 V/cm, the yield decreases rapidly as more and more convoys are swept out of view of the analyzer. A 50 V/cm deflection field eliminates the convoy electrons completely and only Rydberg electrons, ionized by the analyzer field, now contribute to the measured yields. As the strength of the field F_I is increased up to 225 V/cm the measured yield of Rydberg electrons field-ionized in the analyzer decreases more slowly. The decrease results from Rydberg states that are already ionized upstream by the deflection field and therefore no longer contribute to the yield.

The observed shape of the electron cusp also changes as the convoy electrons are prevented from entering the analyzer. If only field ionized Rydberg electrons are detected the cusp shape is completely determined by the analyzer resolution function indicating an electron energy distribution with width $\Delta E/E$ smaller than 0.9%. Figure 16 compares the shape of two electron cusps, one measured with the

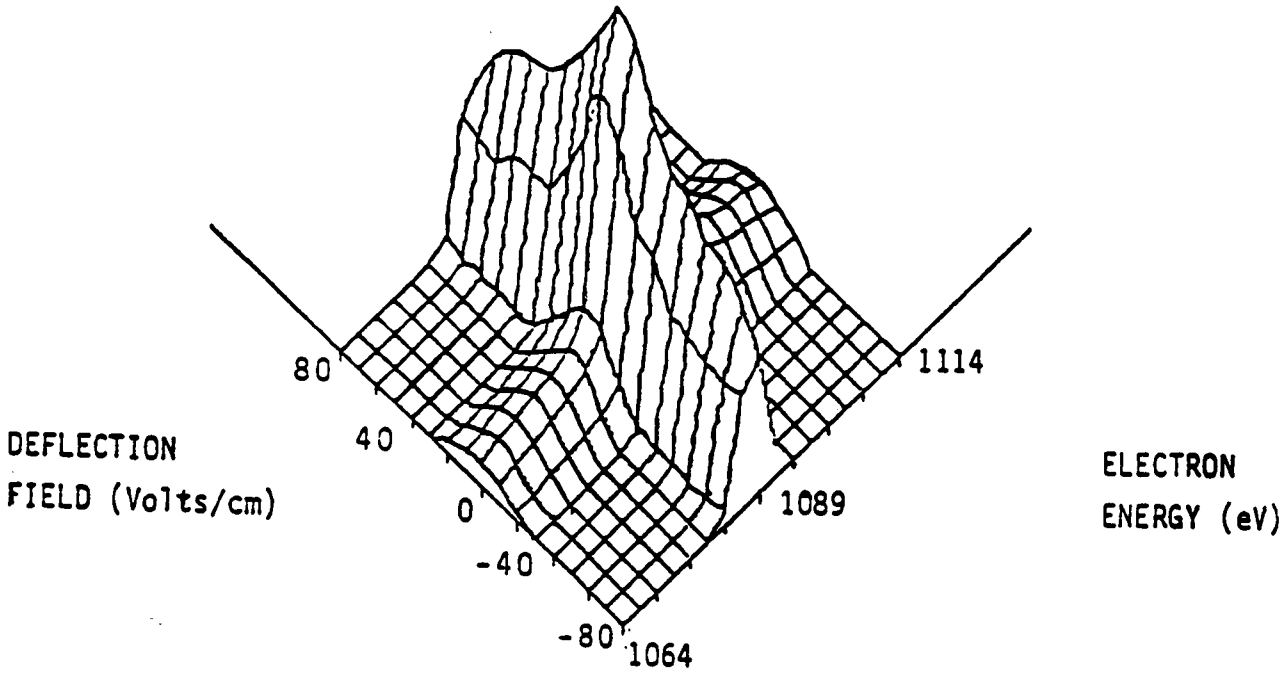

Figure 14. Electron energy distribution as a function of a deflection field F_I applied perpendicular to the beam.

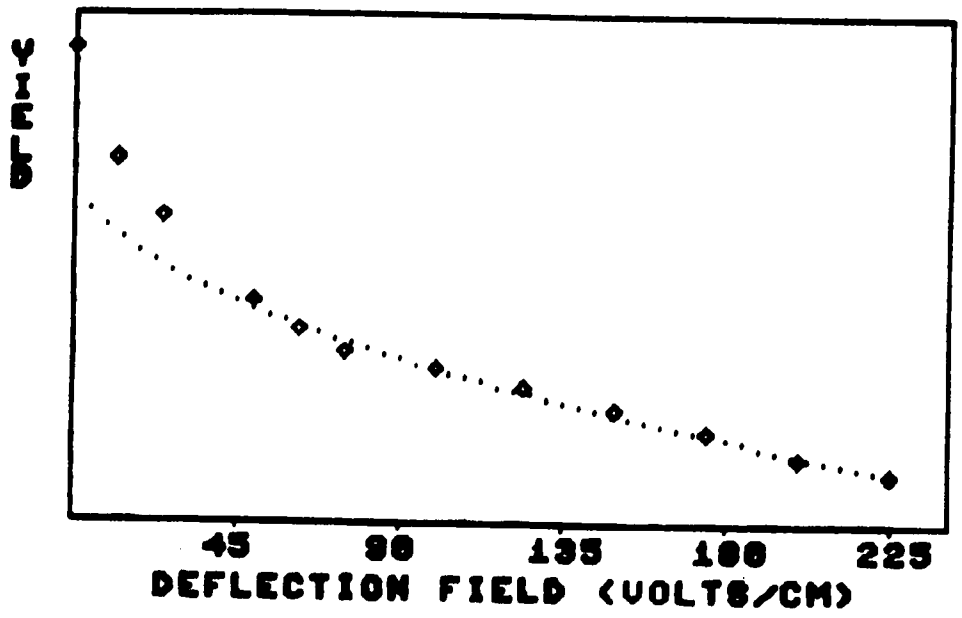

Figure 15. Electron yield from the out of focus target as a function of electric field F_I. The dotted line shows the contribution of analyzer field ionized Rydberg electrons to the measured yield.

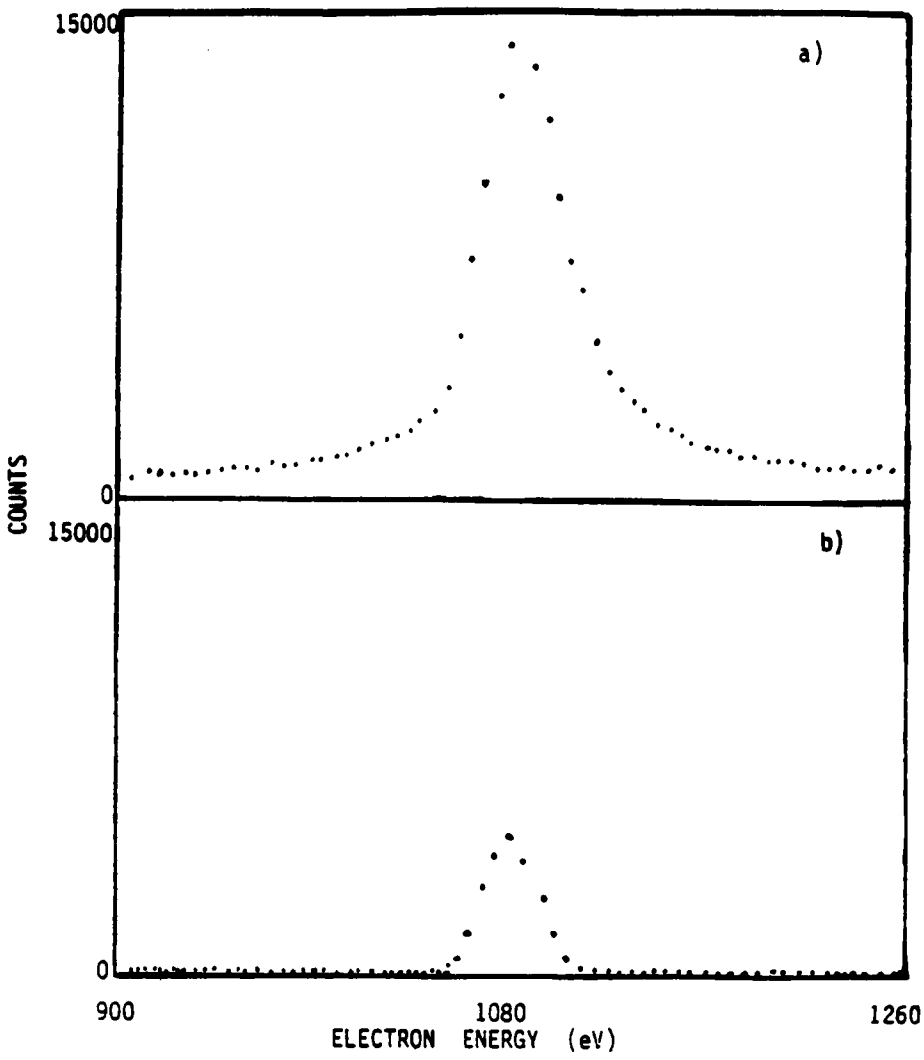

Figure 16. The shapes of two electron cusps measured with a) an electric field F_I = 0 and b) an electric field F_I = 62.5V/cm perpendicular to the beam direction.

field $F_I = 0$ and one with a field $F_I = 62.5$ V/cm perpendicular to the beam direction. The decrease in the yield of Rydberg electrons field ionized in the analyzer, measured as a function of deflection field, can be used to test the initial quantum state population P(n) of the highly excited states exiting the solid target. Passing through the region of the field $F_I \geq 50$ V/cm, the highest Rydberg states are already ionized before the projectiles enter the analyzer field $F_A \cong 450$ V/cm. We only detect Rydberg electrons from states $n_I(F_I) > n > n_A\ (F_A)$. The measured yields are therefore proportional to $\int_{n_A}^{n_I} P(n)dn$. Assuming a classical ionization threshold field $F_c \propto 1/n^4$ and a quantum state population P(n) varying as n^a we use a grid search fitting routine to determine the exponent a.[15,26] For all spectra measured the routine yields $a = -3.00 \pm 0.02$ indicating $P(n) \propto n^{-3}$ for 32 MeV and 18 MeV oxygen ions passing through carbon foils. This method appears to test the well known n^{-3} law expected to hold for n-state populations created by high velocity excitation and capture processes at least as well as any other known method.[27,28]

Using $P(n) \propto n^{-3}$ we extrapolate the contribution of field ionized Rydberg states to the convoy electron yields observed with zero deflection field F_I from the Rydberg electron yields measured with fields strong enough to sweep all convoy electrons out of view of the analyzer. The dotted line in Figure 15 shows the contribution of analyzer field ionized Rydberg electrons to the measured electron yield as a function of the field F_I. For zero field we find that for a target 20 cm upstream from the entrance focus of the analyzer, the ratio of Rydberg electron to convoy electron yield is approximately

2 to 1. However, this implies that for a target more appropriately placed at the entrance focus, the contribution of Rydberg electrons to the convoy electron yield is less than 3%. The out of focus target strongly discriminates against the detection of convoy electrons.

C. A Check on Enhanced Rydberg Electron Yield: Alignment

For 0.75 MeV protons traversing carbon foils, it has been reported by Vager et al. that an electric field perpendicular to the beam direction is much more effective in field ionization of Rydberg states than a field along the beam direction.[16] This was taken as an indication of strong alignment in the excitation, suggesting a highly oblate electron density in the Rydberg states with respect to the beam direction.

It was a goal of our experiments to check for indications of an initial nonstatistical sublevel population for oxygen ions traversing carbon targets. The rotatable ionization plates allowed us to apply a field F_I either perpendicular or along the beam direction. This field was varied from 70 V/cm to 250 V/cm while a constant perpendicular deflection field of 50 V/cm prevented Rydberg electrons ionized between the ionization plates and convoy electrons produced in the target from entering the analyzer. The analyzer field was set to analyze electrons with a velocity equal to the beam velocity. Because all convoys are swept out of view of the analyzer by the 50 V/cm deflection field, only Rydberg electrons ionized by the analyzer field will have this velocity. In Figure 17 the yield of Rydberg electrons ionized in the analyzer as a function of F_I perpendicular and parallel to the beam

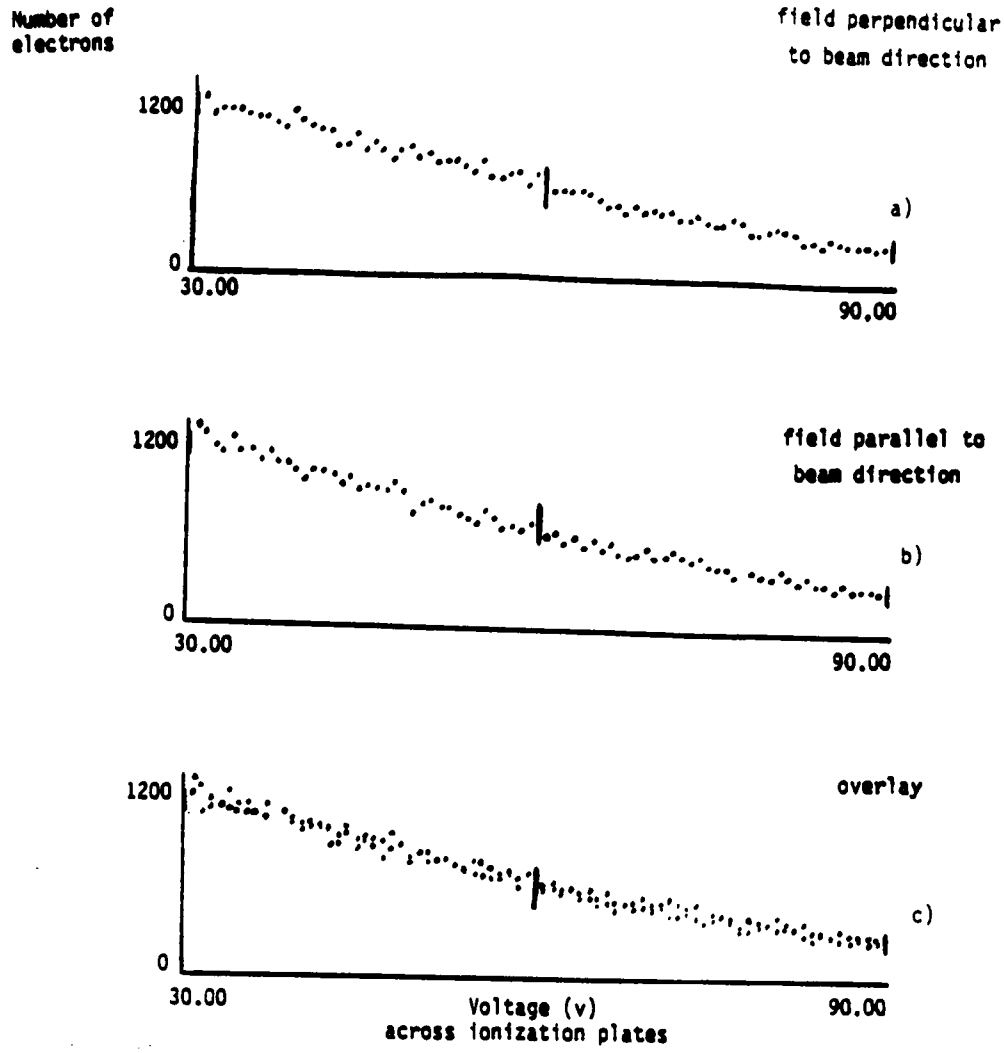

Figure 17. Yield of Rydberg electrons ionized in the analyzer as a function of F_I a) perpendicular and b) parallel to the beam. Both yields are seen in the overlay c).

direction is shown. This yield is measured to be independent of the orientation of the ionization plates.

D. Quantum Beat Oscillations: Coherent Excitation

While making the above measurements oscillations in the Rydberg yield as a function of ionization field, see Figure 17, are observed for both transverse and longitudinal field directions indicating a nonstatistical population. These oscillations are ascribed to coherent excitation of high Rydberg states.

Quantum beats indicating coherent excitation of the manifold of n^2 Stark states associated with each quantum number n have also been observed for hydrogen on carbon foils by Vager et al. and Yamazaki and Oda.[16,30] One can understand these oscillations within the frame work of a simplified model based on the first order perturbation theory.[16,29] The Schroedinger equation for an electron moving in a Coulomb field can be separated in parabolic coordinates. The eigenfunctions are characterized by the parabolic quantum numbers n_1, n_2 and m, and all eigenvalues for eigenfunctions with the same $n = n_1 + n_2 + |m| + 1$ are degenerate if no external field is present. The separability of the Schroedinger equation in parabolic coordinates is maintained in the presence of an external field F, but the degeneracy is removed.

We shall consider the case of one principle quantum number n. Assume that as the projectile passes through the target the manifold of n Stark levels is coherently excited, which means that the wave function describing the state is a superposition of parabolic

eigenfunctions with different n_1 (for simplicity let m = 0 but the same arguments hold for each m). Let $\Psi_n(t)$ be the time (t) dependent wave function for the coherently excited state and let ϕ_{n_1} be the eigenfunction with parabolic quantum number n_1 then

$$\Psi_n(t) = \sum_{n_1=0}^{n-1} a_{n_1}\phi_{n_1}e^{-E_{nn_1}t} \qquad (10)$$

E_{nn_1} is the energy for a state with principal quantum number n and parabolic quantum number n_1. If no field external field is present, we have

$$E_{nn_1} = E_n = \frac{e^2Z}{8\pi\epsilon_0 a_0}(1/n^2) \qquad (11)$$

which is independent of n_1. However in an external field the energy E_{nn_1} is given by

$$E_{nn_1} = \frac{e^2Z}{8\pi\epsilon_0 a_0}(1/n^2) + \frac{3Fea_0n}{2\ Z}(n_1-n_2) \qquad (12)$$

$$= \frac{e^2Z}{8\pi\epsilon_0 a_0}(1/n2) + \frac{3Fea_0n}{2\ Z}(n_1-n+1)$$

$$= \frac{e^2Z}{8\pi\epsilon_0 a_0}(1/n_2) - \frac{3Fea_0n}{2\ Z}(n-1) + \frac{3Fea_0nn_1}{Z}$$

$$= A + \frac{3Fea_0nn_1}{Z}$$

where the term A depends on n while the second term depends on n_1. Thus equation 10 becomes

$$\Psi_n(t) = \sum_{n_1=0}^{n-1} a_{n_1}\phi_{n_1} e^{-i(A/\hbar)t} e^{-i2\pi n_1(3ea_0n/Zh)Ft} \qquad (13)$$

After a fixed time interval Δt the wave function may be written as

$$\Psi_n(\Delta t) = C\sum_{n_1=0}^{n-1} a_{n_1}\phi_{n_1} e^{-i2\pi n_1 f_n F} \qquad (14)$$

Here $C = e^{-i(A/\hbar)\Delta t}$. $\Psi_n(\Delta t)$ is a periodic function of the field strength F with fundamental frequency

$$f_n = \frac{3nea_0\Delta t}{Zh} \qquad (15)$$

or fundamental period

$$\tau = \frac{Zh}{3nea_0\Delta t} \qquad (16)$$

Assume that after this fixed time interval Δt the projectile is entering a region in which the field has a different direction. In our experiment the ionization plates produced a field horizontally perpendicular or parallel to the beam direction while the analyzer produced a field vertically perpendicular to the beam direction. New Stark sublevels are now eigenstates in this new field. The energy of

these sublevel depends on the quantum number $(n_1'-n_2')$. For m=0 the energy depends only on n_1'. If the field is strong enough to ionize states with $n_1' > n_a$ and not strong enough to ionize states with $n_1' < n_a$ and if the sublevel χ has $n_1' > n_a$, then it can be ionized by the field. The probability that ionization occurs is proportional to the probability that a measurement at the fixed time t yields eigenvalues corresponding to χ. This probability is proportional to the square of the overlap integral $|\langle\chi|\Psi_n(\Delta t)\rangle|^2$. Thus we have

$$|\langle\chi|\Psi_n(\Delta t)\rangle|^2 = |\sum_{n_1} a_{n_1}\langle\chi|\phi n_1\rangle e^{-i2\pi n_1 f_n F}|^2 = |\sum_k C_k e^{-i2\pi k f_n F}|^2 \quad (17)$$

$$= \sum_{kk'} C^*_k C_{k'} e^{i2\pi(k-k')f_n F}$$

This overlap integral is a periodic function of F with fundamental period τ. The ionization probability is therefore a periodic function of F with fundamental period τ. Since $\tau = Zh/3nea_0\Delta t$ is proportional to Z we expect to observe oscillations with larger periods for larger Z values. The period of the oscillation also depends on Δt, thus the shorter Δt is the larger the period will be.

In our experiments $\Delta t = \ell/v$ is the time spent in the ionization field whose effective length is ℓ. The most probable charge state for a 32 MeV oxygen ion exiting a Carbon foil is q = 7. If we assume that this also holds for highly excited states, then most of the Rydberg states leaving the foil are hydrogen-like and the effective nuclear charge is Z = 8. Using the most probable charge state of the ion after

the foil q = 7 we estimate n for the lowest state ionized by the analyzer field from the classical ionization threshold neglecting Stark splitting $E_A = 3.2 \times 10^8 Z^3/n^4$. Here Z = q+1 = 8. We calculate τ = 7.9 V/cm for ℓ = 38 mm. Simple inspection of the spacings between successive minima in independently measured yield curves of the type displayed in Figure 18 is already sufficient to yield $\tau = 7.5 \pm 0.5$ V/cm. With three different ionization field lengths, ℓ = 4mm, 12mmm and 38mm, we confirm that τ scales as ℓ^{-1}. Higher harmonics have already been observed when the ionization field region is kept short. Our results confirm coherent excitation of high Rydberg states as a result of the interaction of fast oxygen ions with carbon foils. Using continuation across the ionization limit we expect coherences to persist in the low lying convoy electron continuum as well.[30]

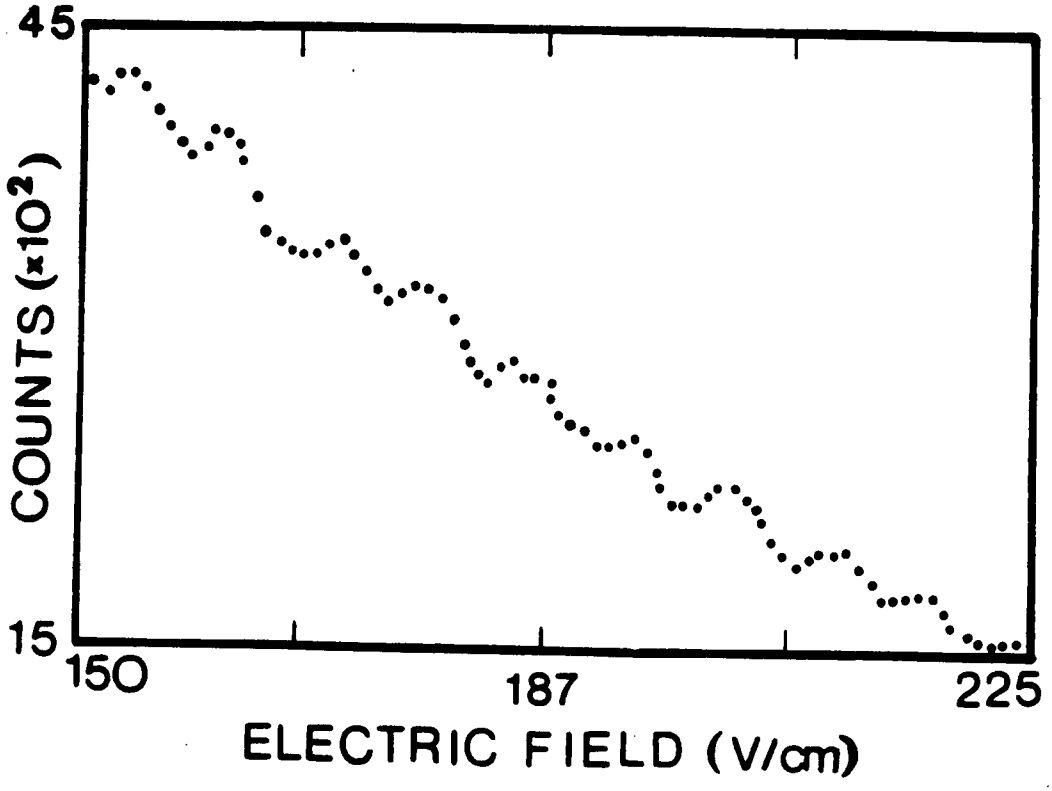

Figure 18. Oscillations in the Rydberg yield as a function of ionization field F_I.

Chapter IV

Discussion

A. Current Dispute Examined

The primary motivation for this thesis, as stated in Chapter 1, is to determine quantitatively the contribution of field ionized Rydberg electrons to traditionally convoy electron energy distributions for 18MeV O^{3+} and 32MeV O^{5+} ions on carbon foils.

Vager et al. have reported that for H^+, He^+, and Ne^+ projectiles on carbon foils, that atoms or ions in high Rydberg states and convoy electrons emerge with comparable probabilities.[20] They have suggested that field stripping of these high Rydberg states inside the electron analyzer is the source of a significant fraction of the detected electrons, even for heavy ion projectiles. Our investigations show unambiguously that the fraction of electrons from high Rydberg states which contaminate our traditionally measured convoy electron spectrum is small (3%).

The experimental setup used by Vager et al. is shown in Figure 19. Their foil target is placed approximately 16cm away from the entrance focus of a 30° electrostatic electron analyzer, in contrast to the traditional placement of foil target directly in the entrance focus of an analyzer (see Figure 6). The out of focus target strongly discriminates against the detection of convoy electrons.

Vager et al. find that the contribution of Rydberg electrons field ionized in the analyzer to their measured electron energy distribution is of the same order of magnitude as that of convoy electrons. This

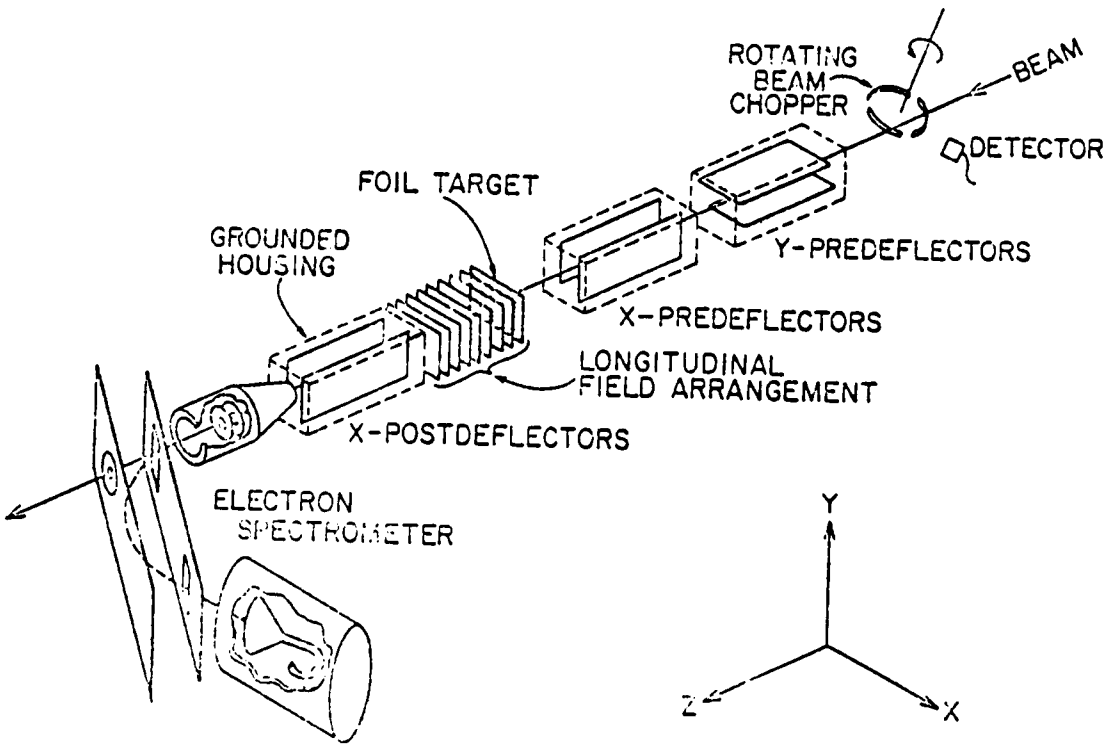

Figure 19. Experimental setup used by Vager et al.

Source: Z. Vager, B. J. Zabransky, D. Schneider, E. P. Kanter, Gu Yuan Zhuang, and D. S. Gemmell, Phys. Rev. Lett. 48, 592 (1982).

agrees with our measurements for oxygen ions on a target 20cm upstream from the entrance focus of our analyzer. However, in the interpretation of their experimental results, which were obtained with such an out of focus target only, Vager et al. did not take into account the extreme reduction of the acceptance angle of their electron energy analyzer and incorrectly concluded that all convoy cusps are severely contaminated by field stripped Rydberg electrons.

Our measured ratio of Rydberg electron to convoy electron yield of approximately 2 to 1 for the out of focus target implies that for a target more appropriately placed at the entrance focus, the contribution of Rydberg electrons to the convoy electron yield is less than 3%.

B. Quantum State Population P(n)

The mechanism responsible for the production of highly excited states by fast heavy ions passing through a foil target is not well understood at this writing and several models are proposed. While some investigators argue for last layer OBK type electron capture or lastlayer bound-bound excitation processes, others suggest a multi-step model for the production processes of the projectile electrons.[29,7] Different models predict different distributions of the electrons among the many possible highly excited states that are available. Knowledge of the quantum state population P(n) of these high Rydberg states can offer clues as to what production mechanism is predominately at work. All our measurements are consistent with a quantum state population P(n) varying as n^{-3} which is predicted for OBK type capture or bound-

bound excitation processes in the last layer. However these processes predict population of low ℓ states only, and Betz et al. report that high angular momentum states are heavily populated. Thus no conclusions can be drawn which directly favor any one of the available models at the expense of the others. Additional in depth studies of these foil excited Rydberg states are necessary before the production mechanisms are revealed.

C. Nonstatistical Sublevel Populations

The indication of strong alignment in the excitation of Rydberg states, reported for protons on carbon foils by Vager et al. was not found in our experiment, where we compared the effectiveness in field ionization of Rydberg states of an electric field perpendicular to the beam direction with that of a field along the beam direction (see Figure 17). All our results are for oxygen ions on carbon foils.

However we observed oscillations in the Rydberg yield as a function of ionization field, as shown in Figure 18, for both transverse and longitudinal field directions indicating a nonstatistical population. These oscillations are ascribed to coherent excitation of high Rydberg states. Rotating the field direction can strongly influence the ionization probability in a narrow band of n states near the classical ionization limit only. All n states above this narrow band will ionize rapidly independent of field direction. The oscillation amplitude in Figure 18 lets us estimate the magnitude of the contribution of this narrow band to the total signal as a function of F_I and we therefore suspect that the magnitude of the

effect of changing the field direction on the Rydberg electron yield reported by Vager et al. is unphysically large.

LIST OF REFERENCES

LIST OF REFERENCES

1. J. Remillieux, J. C. Poizat, M. J. Gaillard, Proc. of the 9th Int. Conf. on "Atomic Collisions in Solids" Lyon/France, July 1981 (ed. J. Remillieux, J. C. Poizat, M. J. Gaillard).

2. J. Davidson, W. S. Bickel, Nucl. Instrum. Methods 110, 255 (1973).

3. D. Kleppner, M. G. Littman and M. L. Zimmerman, Sci. Am. 5, 244 (1981).

4. A. C. Rivere, Methods of Experimental Physics (Academic, New York, 1968).

5. H. D. Betz, D. Roschenthaler, J. Rothermel, Phys. Rev. Lett. 50, 34 (1983).

6. H. D. Betz, J. Rothermel, D. Roschenthaler, F. Bell, R. Schuch and G. Nolte, Phys. Lett. 91A, 12 (1982).

7. H. D. Betz, in Lecture Notes in Physics. 213, edited by K. O. Groeneveld, W. Meckbach and I. A. Sellin, (Springer, Berlin, 1984), p. 115.

8. R. F. Stebbings, C. J. Latimer, W. P. West, F. B. Dunning, and T. B. Cook, Phys. Rev. A 12, 1453 (1975).

9. A. F. J. Van Raan, G. Braun, and W. Raith, J. Phys. B 9, L173 (1976)

10. D. Kleppner, Atomic Physics. Vol 5, Proceedings of the Fifth International Conference on Atomic Physics, edited by R. Marrus, H. A. Shugart, and M. H. Prior, (Plenum Press, New York, 1977).

11. D. Kleppner,M. G. Littman and M. L. Zimmerman, in Rydberg States of Atoms and Molecules, edited by R. F. Stebbings and F. B. Dunning (Cambridge University, New York, 1983), p. 312.

12. T. W. Ducus, M. G. Littman, R. R. Freeman, and D. Kleppner, Phys. Rev. Lett. 35, 366 (1975).

13. M. G. Littman, M. M. Kash, and D. Kleppner, Phys. Rev. Lett. 41, 103 (1978).

14. W. E. Cooke and T. F. Gallager, Phys. Rev. A 17, 1226 (1978).

15. H. A. Bethe and E. A. Salpeter, Quantum Mechanics of One and Two Electron Atoms (Academic, New York,1957).

16. Z. Vager, E. P. Kanter, D. Schneider, and D. S. Gemmell, Phys. Rev. Lett. 50, 954 (1983).

17. M. Breinig, S. B. Elston, S. Huldt, L. Liljeby, C. R. Vane, S. D. Berry, G. A. Glass, M. Schauer, I. A. Sellin, G. D. Alton, S. Datz, S. Overbury, R. Laubert, and M. Suter, Phys. Rev. A 25, 3015 (1982)

18. I. A. Sellin, S. D. Berry, M. Breinig, and C. Bottcher, in Lecture Notes in Physics. 213, edited by K. O. Groeneveld, W. Meckbach and I. A. Sellin (Springer-Verlag, Berlin, 1984), p.109.

19. Y. Yamazaki and N. Oda,Phys. Rev. Lett. 52, 29 (1984).

20. Z. Vager, B. J. Zabransky, D. Schneider, E. P. Kanter, Gu Yuan Zhuang, and D. S. Gemmell, Phys. Rev. Lett. 48, 592 (1982).

21. M. W. Lucas and J. Macek, Phys. Rev. Lett. 50, 1014 (1983).

22. I. B. E. Nemirovsky, W. Meckbach, and P. Focke, Phys. Rev. Lett. 50, 1015 (1983).

23. M. Breinig, S. B. Elston, S. D. Berry, G. A. Glass, I. A. Sellin, and R. Vane, Phys. Rev. Lett. 50, 1016 (1983).

24. K. D. Sevier, Low Energy Electron Spectrometry (Wiley-Interscience, New York, 1972).

25. G. A. Glass, Electron Capture to the Contiuum from Atomic Hydrogen. Thesis, The University of Tenessee (1984).

26. P. R. Bevington, Data Reduction and Error Analysis for thr Physical Sciences (McGraw-Hill, New York, 1969).

27. M. E. Rudd and J. Macek, Case Stud. Atom. Phys. 3, 125 (1972).

28. M. Rodbro and F. D. Anderson, J. Phys. B 12, 2883 (1979) and references therein.

29. E. P. Kanter, D. Schneider, Z. Vager, D. S. Gemmell, B. J. Zabransky, Gu Yuan Zhuang, P. Arcuni, P. M. Koch, D. R. Mariani, W. Van Water, Phys. Rev. A 29, 583 (1984).

30. J. Burdorfer, in Lecture Notes in Physics 213, edited by K. O. Groeneveld, W. Meckbach and I. A. Sellin (Springer, Berlin 1984) p. 32.

VITA

Peter Paul Engar, Jr was born in Mahattan, New York on July 8, 1955. He graduated from Valley Stream High School in 1973 and attended Nassau Community College where he received a Associate of Arts degree in Liberal Arts. The degree was awarded in December 1975.

In the winter of 1976 he entered the State University of New York at Stony Brook. In August 1979 he received a Bachelor of Science degree in Physics. Starting in the fall of 1979 he accepted a teaching assistantship, for three semesters, at the College of William and Mary.

Since September of 1981 he attended the Graduate School of The University of Tennesee, Knoxville and worked towards a Master's degree in experimental Physics. He was awarded this degree in August of 1985. Mr. Engar will be employed at Kansas State University as a assistant staff scientist.